LIQUID-INTERFACE ORIENTATION-DICTATED SELF-ASSEMBLY OF COLLOIDAL SEMICONDUCTOR NANOCRYSTALS AND ITS APPLICATIONS

A THESIS SUBMITTED TO

THE GRADUATE SCHOOL OF ENGINEERING AND SCIENCE

OF BILKENT UNIVERSITY

IN PARTIAL FULFILLMENT OF THE REQUIREMENTS FOR

THE DEGREE OF

MASTER OF SCIENCE

IN

PHYSICS

By

Mohsin Waris

August 2023

Liquid-Interface Orientation-Dictated Self-Assembly of Colloidal Semiconductor Nanocrystals and its Applications
By Mohsin Waris
August 2023

We certify that we have read this thesis and that in our opinion it is fully adequate, in scope and in quality, as a thesis for the degree of Master of Science.

Hilmi Volkan Demir(Advisor)

Won Mi Ahn

Yusuf Keleştemur

Approved for the Graduate School of Engineering and Science:

Orhan Arikan
Director of the Graduate School

ABSTRACT

LIQUID-INTERFACE ORIENTATION-DICTATED SELF-ASSEMBLY OF COLLOIDAL SEMICONDUCTOR NANOCRYSTALS AND ITS APPLICATIONS

Mohsin Waris
M.S. in Physics
Advisor: Hilmi Volkan Demir
August 2023

Over the past, different techniques have been used for the self-assembly of nanocrystals (NCs). Recently, the orientation control over the assembly of anisotropic NCs has been achieved using liquid-interface self-assembly, which is a simple yet vastly applicable technique. Here, we propose and show the first account of the application of this method to assemble multi-layered alternating-orientation NC films, with distinct orientation control of our choice over the NCs in each layer. Being laterally atomically flat, these anisotropic NCs belong to a class of quasi-two-dimensional nanocrystals with one confined dimension. Exhibiting extraordinarily large absorption cross-sections, ultra-narrow emission linewidths, and intrinsic structural anisotropy, these nanoplatelets (NPLs) possess characteristics comparable to those of epitaxially grown quantum wells, though while offering low-cost solution-based synthesis and processability at the same time. Due to this anisotropy, the emission of these NPLs is directional with mostly in-plane transition dipole moments, making them favorable for a variety of optoelectronic active media with orientation control over their deposited films. To achieve this, we have assembled the NPL films with one defined orientation and successfully attained their orientation control using macroscopic parameters, including the evaporation rate of the solvent and subphase selection to be used as the active layers for a number of optoelectronic devices. We demonstrated different multi-layered structures of these NPLs with varying orientations. The resulting surface roughness in all these films was successfully kept, on average, with S_q smoother than 2 nm. We further extended this self-assembly technique to different classes of nanocrystals including large hexagonal NPLs (with around 100 nm in lateral dimensions) and cubic quantum dots (with around 15 nm on each side) to show the versatility of our method. The findings of this thesis indicate that our orientation-dictated self-assembly approach holds great promise for

constructing complex colloidal structures made of these oriented nanocrystals as the building blocks.

Keywords: Nanocrystals, nanoplatelets, liquid-interface self-assembly, orientation control.

ÖZET

KOLOİDAL YARIİLETKEN NANOKRİSTALLERİN SIVI-ARAYÜZEY YÖNLENDİRMELİ ÖZ-DİZİLİMİ VE UYGULAMALARI

Mohsin Waris
Fizik, Yüksek Lisans
Tez Danışmanı: Hilmi Volkan Demir
Ağustos 2023

Geçmişte, nanokristallerin (NK'ler) kendi kendine dizilmesi (öz-dizilim) için farklı yöntemler kullanılmıştır. Son zamanlarda, anizotropik NK'lerin dizilimi üzerindeki yönlendirme kontrolü, basit ama oldukça uygulanabilir bir teknik olan sıvı arayüzlü öz-dizilim kullanılarak elde edilmiştir. Burada, her katmandaki NK'ler üzerinde tercih ettiğimiz farklı yönlendirme kontrolü ile çok katmanlı alternatif yönelimli NK filmleri birleştirmek için bu yöntemin uygulanmasının ilk açıklamasını öneriyor ve gösteriyoruz. Atomik seviyede düz olan bu anizotropik NK'ler, bir sınırlı boyuta sahip, hemen hemen iki boyutlu nanokristal sınıfına aittir. Olağanüstü derecede büyük soğurma kesitleri, son derece dar ışıma genişlikleri ve yapısal anizotropi sergileyen bu nanolevhalar (NL'ler), epitaksiyel olarak büyütülmüş kuantum kuyularınınkine benzer özelliklere sahiptir, aynı zamanda düşük maliyetli, çözelti tabanlı sentez ve işlenebilirlik sunar. Bu anizotropi nedeniyle, nanolevhaların ışıması çoğunlukla düzlem içi geçiş dipol momentleri ile yönlüdür, bu da onları, biriktirilen filmleri üzerinde yön kontrolü olan çeşitli optoelektronik etkin ortamları için uygun hale getirir. Bunu başarmak için, nanolevha filmlerini tanımlanmış bir yönelimle bir araya getirdik ve bir dizi optoelektronik aygıt için etkin katmanlar olarak kullanılacak çözücünün buharlaşma oranı ve alt faz seçimi dahil olmak üzere makroskobik parametreleri kullanarak yönlendirme kontrollerini başarıyla elde ettik. Nanolevhaların farklı çok katmanlı yapılarını değişen yönelimlerle gösterdik. Tüm bu filmlerde ortaya çıkan yüzey pürüzlülüğü (S_q), ortalama 2 nm'den daha pürüzsüz olacak şekilde elde edildi. Yöntemimizin çok yönlülüğünü göstermek için bu öz-dizilim yöntemini, büyük altıgen nanolevhalar (yanal boyutlarda yaklaşık 100 nm) ve kübik kuantum noktaları (her bir tarafta yaklaşık 15 nm) dahil olmak üzere

farklı nanokristal sınıflarında uyguladık. Bu tezin bulguları yönelime dayalı öz-dizilim yaklaşımımızın, yapı taşları olarak bu yönlendirilmiş nanokristallerden yapılmış karmaşık koloidal yapıların inşa edilmesi için büyük umut vaat ettiğini göstermektedir.

Anahtar sözcükler: Nanokristaller, nanoplateletler, sıvı-arayüz öz-dizilimi, oryantasyon kontrolü.

Acknowledgement

After completing my BS in Physics from my home country, Pakistan, I decided further to pursue my studies at the Master's level to dig down further in the field. The acceptance from Bilkent University on a full bright scholarship was no less than a dream, and that too at the time of COVID-19. So, I would like to thank Bilkent University for providing me with an opportunity and platform to excel in my academic career.

As an international student, it seemed difficult to survive in an unknown environment until I arrived at the Bilkent campus. The hurdles as an MS student were different in terms of online study platform, but once again, thanks to Bilkent University and the Professors of the Physics Department, especially Prof. Hilmi Volkan Demir (for research opportunities), Prof. Ceyhun Bulutay, Prof. Cemal Yalabik and Professor Oguz Gulseren (Department Chair) for providing a fair and best possible environment to the students to learn advanced courses in those difficult days.

My academic journey took a new turn when I got an opportunity to be a part of Prof. Demir's Research group. I thank Prof. Hilmi Volkan Demir for providing excellent research opportunities to a student with little lab research experience like me. Above that, the positive learning environment he and his team provided needs to be appreciated. Apart from being an excellent PI, I would also like to thank Prof. Hilmi Volkan Demir for being nice to me and his other research team members by taking care of even their non-academic stuff.

Further, I wish to thank my jury members, Asst. Prof. Won Mi Ahn and Asst. Prof. Yusuf Keleştemur (METU) for their precious time in reading my thesis and providing me with feedback.

I would like to express my warmest thanks to our group members who helped me start my research journey and learn basic and advanced lab techniques, especially İklim Yurdakul, Rumon Miah, Farzan Shabani, Furkan Işık, Dr. Betül Canımkurbey, Dr. Savaş Delikanlı, Rabia Önen, Özgün Akyüz, Dr. Mojtaba Sadeghi, and some of our previous group members, Dr. Satish Kumar, Dr. Muhammad Ibrahim, Mohammad Ahmad, and Dr. Zeynep Dikmen. It is never

easy for international students to survive abroad until they encounter people who become their family over time. so I want to express a warm thanks to my Bilkent family, especially Ali Sheraz, Dr. Iqra Munir, Dr. Salahuddin Zafar, Hafiz Muhammad Shakir, Zohaib Kayani, Muhammad Jawad, Faiqa Nazir, Osama Adil, Sayoon Gill and Sufyan Ali.

Lastly, I think I am liable to acknowledge and must not forget to mention the names of those who are always among the happiest people in my success, the ones who have brought me up with love and care, those who have fulfilled my dreams, who have to bear me with my goods and bads, the ones who have passed through toughs to see me excelling, taught me since my childhood, and guided me in every field of life, they are my family members. So I would like to express my deepest love to Mr. Waris Ali Sajid (father), Ms. Farah Waris (mother), Dr. Sheikh Abdul-Rahman Abbasi (mentor), Anas Waris, Huma Anas, Sadaf Waris, Moazzam Ali Tahir, Hera Waris, and my special and dearest younger brother Abdul Samad Waris.

Contents

List of Figures

List of Tables

Chapter 1

Introduction

Colloidally synthesized semiconductor nanocrystals, abbreviated as NCs, are playing a significant role in the field of colloidal nanophotonics and have advanced the field since their birth, almost three decades ago. These NCs exhibit exciting optoelectronic properties that can be controlled by varying the particle's dimensions [1], [2].

With the passage of time, the advances in the realm of colloidal synthesis techniques have allowed to study different physiochemical properties of NCs, including chemical composition and shapes, which resulted in the production of highly emissive NCs with spectrally narrow emission bands, in the range of the whole visible spectrum. Presently, the state-of-art technique enables the synthesis of colloidal NCs with attractive characteristics of monodispersity and near unity Quantum Efficiency and, hence making NCs with well-controlled shapes and compositions suitable for devices as lasers [3], [4] LEDs [5], [6] and displays [7].

In terms of dimensionality, these NCs can be grouped into different classes like quantum dots, quantum rods, or quantum wells. The most recent addition to these NC classes is quasi-two-dimensional (quasi-2D) colloidal quantum wells (CQWs). These NCs are atomically flat, with precise vertical thickness control making it a 1D confined structure [8], [9]. They exhibit similar properties

to the quantum wells grown epitaxially, yet they are more advantageous in that they are produced with low-cost synthetic techniques. CQWs, or alternatively commonly nicknamed nanoplatelets (NPLs), exhibit exceptional properties such as extremely-narrow emission linewidth [9], [10] giant oscillator strength [9] enhanced optical absorption [11] and in-plane dipole moments [12] resulting in directional emission [13]. The planar distribution of dipoles in these CQWs display optical anisotropy and makes them anisotropic emitters with mostly out-of-plane emission, with respect to the plane of nanoplatelets. Exploiting this property, one can obtain directional emission with controlled orientation of these CQWs in solid films. If achieved, this can be very useful in lighting devices where directionality plays an important role in LEDs and displays, and can enhance operational efficiencies [14]. The challenge comes in the controlled orientation in the assembly of these NPLs in the whole solid deposited film, which must be achieved to achieve directional emission.

There are a lot of techniques that can be used to deposit solid films of these NPLs including drop casting and spin-coating, but they often result in mixed orientation of NPLs resulting in the mixture of two phases which is not desired. Here mixed phases are referred to the orientations of these NPLs which are face-down, and edge-up, that is, nonstacked and stacked, respectively [15]. This obstructs the utilization of optical anisotropy in NPLs and thus shows the significance of orientation control of these NPLs in solid-deposited films in optoelectronic devices. Therefore, the thin film deposition of these NPLs is an important step in the device fabrication process.

As NCs are employed as an active layer in optoelectronic devices, it is often required to have a certain film thickness and adequate uniformity. To do so, researchers have commonly opted the deposition techniques of spin-coating or drop casting. In the spin coating, a certain amount of optimized solution of NCs is dropped on a substrate, which is rapidly rotating at a pre-set speed. This approach deposits the material, when properly applied, with required thickness and uniformity, to some extent, but results in mixed orientation. The later technique requires a drop of NCs solution to be dropped on a substrate with controlled

drying, which allows for the optimum thickness of film but suffers non-uniformity due to irregular thickness resulting from mixed orientations and the presence of multilayer of NCs at some parts of the substrate. Therefore, it is quite difficult to obtain precise thicknesses of films prepared by both methods, as a lot of factors affect the quality of the deposited films (e.g., NCs concentration, dropping amount, drying criteria), and so these factors must be well controlled. Furthermore, neither of these techniques allows the orientation control of NPLs; therefore, an alternative method must be used for the oriented deposition of NC films.

To enable a better control of film thickness, advanced techniques such as layer-by-layer depositions or Langmuir-Blodgett (LB) are employed, and both offer excellent control over film thickness and so are considered high-precision deposition tools. Similarly, such liquid-air interface self-assembly deposition techniques were employed for QDs [16], [17] and nanorods (NRs) [18], [19]. Despite being excellent techniques for thickness-controlled depositions, very few studies were reported for the deposition of Cd-based NPLs [20], but comparatively more for Cd-based QDs have been reported [21]–[23]. There are still many independent factors on which the quality of film depends, in terms of the film thickness, in these methods. Furthermore, to study the optical properties of such NPL films in one specific orientation, as face-down or edge-up mentioned earlier, it is quite difficult to opt LB method for Edgeup depositions which makes their studies and implementation in devices further challenging.

To develop a deeper insight into the properties of self-assembled films of NCs, we must look for techniques that should not be limited to the self-assembly of these NCs but also allow us to control the orientations. A recent and simple technique employed for the oriented self-assembly of NPLs is liquid-liquid interface self-assembly [13] in which NPLs dispersed in a non-polar solvent are dropped over a polar solvent, known as subphase, with orientation being controlled by the evaporation rate of the solvent in which NPLs are dispersed [24]. Apart from minor factors such as optimizing the concentration and dropping amount of NPLs, the evaporation rate of solvent and selection of subphase is the major factor dictating the orientation and self-assembly of NPLs. There are other liquid-liquid interface

self-assembly methods, too, that have exploited other ways to orient NPLs such as adding surfactants to alter inter-NPL and NPL-subphase interaction potentials [13] and obtain the desired orientations, but adding additives affects the purity of thin films which in turn affects device performance, and hence showing another advantage of exploiting evaporation rate of solvent to orient NPLs in a desired orientation. Talking about the significance of the film quality, in terms of the orientation control and the purity of films, one needs to understand that it is directly related to the performance of lighting devices. Since the electron transmission between device layers is regulated by the hopping process, which is reliant on the atomic-scale spacing between layers and, therefore, on the smoothness of the emissive layer of the device [25]. Consequently, fine control over the orientation and thickness of NPLs in the assembly defines the quality of self-assembled films. Therefore, having a simple yet controlled assembly technique would be indeed very beneficial and advantageous for optoelectronic devices.

Next, we will discuss how we have exploited this self-assembly technique for different NCs in devices in the next chapters.

1.1 Motivation of this Thesis

The objective of this thesis is to exploit the liquid-liquid interface orientation-dictated self-assembly technique for NCs of different sizes and shapes, covering a wide range from CQWs and large hexagonal NPLs to cubic QDs. We have also used this technique to orient CQWs in a desired orientation and formed fixed orientation multilayered and alternating orientation layered structures of CQW films in devices such as LEDs and photodetectors. We have analyzed the optical properties of these films using back focal plane imaging and angular fluorescence response along with the optical properties of the synthesized solution using absorption and photoluminescence spectra. Furthermore, layer-by-layer analysis, the surface smoothness of each layer in the multilayered structure has been systematically evaluated using AFM to understand the relation of device performance to the structure of the active layer. Alongside this, SEM analysis has

been carried out to understand the topologies of the structures formed. Using this oriented self-assembly technique can be further exploited to form self-assembled structures with enough optical gain in the form of amplified spontaneous emission (ASE) from either CQWs or cubic QDs and allowing us to use, study and analyze self-assembled 2D or 3D superstructures in NC based optoelectronic devices.

1.2 Outline of the Thesis

We will now proceed to the next chapters by initially introducing the essential scientific background of the thesis. Therein, we will first introduce colloidal semiconductors, followed by colloidal nanocrystals and their self-assembly. Chapter 3 will cover in-depth information on the materials majorly used in this thesis, which include 4 monolayers (ML) cadmium selenide in the form of core, and core/shell, with initially discussing its synthesis and characterization. Furthermore, we will also cover the self-assembly of these NCs and present some other commonly used liquid-liquid interface self-assembly techniques. In the 4^{th} chapter, we will present the results of the self-assembly experiments with their SEM images, AFM plots, and BFP analysis for the 4ML core/shell films of defined orientation. In Chapter 5, we will present the conclusion along with recommendation for some possible future work.

Chapter 2

Scientific Background

2.1 Colloidal Particles

In the most general sense, colloids are defined as a mixture of two substances, with one substance being dispersed or suspended throughout the other. These two substances can be in different phases of matter. They are also known as two-phase systems of matter. More commonly, colloidal particles are known as solid particles suspended in a liquid (or gaseous) phase [26]. The size of these particles usually lies from some nanometers to several micrometers, making them small enough to be able to stay suspended in the fluid by thermal motion. Some examples of colloids with different combinations of phases are given in (Table 2.1). A mixture is indeed classified as a colloid if the suspended particles in it do not settle at the bottom of the container, when the system is left undisturbed. Such colloidal solutions exhibit Tyndall or Faraday-Tyndall effect, i.e., a phenomenon in which an incident beam of light is scattered when passed through a colloidal system due to the suspended colloidal particles that individually act as scatters [27]. Furthermore, under advanced microscopes, it is seen that the particles are continuously moving in random paths, although suspended, and thus executing Brownian motion. This is a general introduction to the colloidal systems. In the next chapters, we will discuss a class of these colloidal systems known as colloidal

Phase 1		Dispersed Phase (Phase 2)		
Dispersion Medium	**Gas**	**Gas** Not many of examples of these colloids are known, apart from He-Xe under specific conditions [28]	**Liquid** Liquid Aerosols such as clouds, e.g., mist and steam.	**Solid** Solid Aerosols such as ice clouds and smoke.
	Liquid	Foam E.g., whipped cream and shaving cream.	Emulsion E.g., milk and biological membranes.	Sol E.g., pigmented ink, sediments and *colloidal nanocrystals*
	Solid	Solid foam E.g., aerogel, polystyrene etc.	Gel E.g., jelly and bimolecular condensates.	Solid sol E.g., cranberry glass

Table 2.1: Examples of different combinations of phases for colloids.

semiconductor nanocrystals, which is directly related to our thesis work.

2.2 Quantum Confinement Effect

Most of the materials typically intrinsically exist in 3D or bulk form, whereas the confinement effect in some of those materials occurs, as the word suggests when they are made very small such that they are comparable to the de-Broglie wavelength of the electron [29]. In nanocrystals, this is significantly dependent on the material properties, majorly the Bohr radius aB and so the material experiences the confinement effect. In semiconductor nanocrystals, it is the separation between the electron and hole, called as exciton Bohr radius, which has to be comparable to the wavelength of an electron to lead to the quantum confinement

effects. In general, this phenomenon occurs when either of the dimension is 10 nm in length. This decrease in size changes the energy spectrum from continuous to discrete [30] and thus altering and enhancing optical properties. A simple illustration of this phenomenon can be seen from the energy levels of "particle in a box," model, i.e., how the size of the box affects its energy spectrum. For simplicity, we are considering a particle in an infinite potential well, confined in 1D and free in all other two dimensions [31]. Considering this example would be logical to some extent as an electron in a crystal experiences periodic potential wells but with finite barrier. In the case of infinite barriers, the energy is given as

$$E_n = \frac{n^2 h^2}{8mL^2} \tag{2.1}$$

where n is the quantized energy level, h is Planck's constant, m is the mass of the particle, and L is the size of the well. With all these, the separation between the first two successive energy levels is given as

$$E_1 = \frac{h^2}{8mL^2} \quad for \quad n = 1 \quad and \quad E_2 = \frac{4h^2}{8mL^2} \quad for \quad n = 2 \tag{2.2}$$

For example, if we change the size of the well to 2L, the energy spectrum will change as

$$E_1^{"} = \frac{h^2}{8m(2L)^2} = \frac{0.25h^2}{8mL^2} \quad for \quad n = 1 \quad and \quad E_2^{"} = \frac{4h^2}{8m(2L)^2} = \frac{h^2}{8mL^2}, \quad n = 2 \tag{2.3}$$

Here note that E" represents energy for the well with width 2L.

Comparing Equations 2.2 and 2.3, we can see that $E_2" = E_1$, and hence changing the size of the well modifies the energy spectrum and, therefore, the emitted light from such systems. To obtain a complete picture of the energy spectrum, we must take into account the potentials present in the system, which will change the solution of the Schrödinger equation, from where we obtain the energy-momentum relations and the corresponding spectra.

As we have talked about the impact of varying confined dimensions on energy spectra roughly, we now must look at different species produced when we confine a certain dimension. The bulk materials are considered 3D materials, and if we

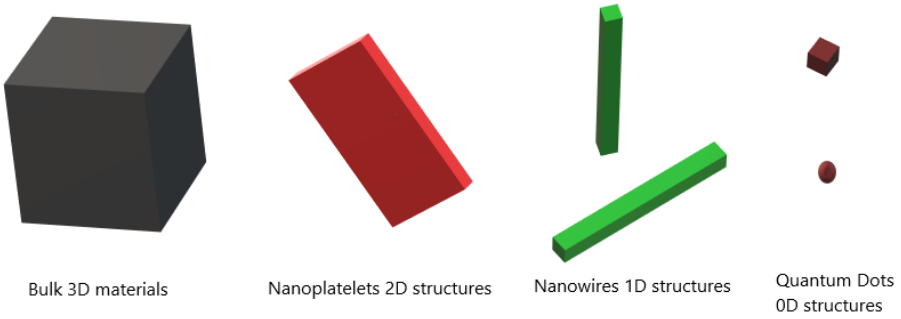

Figure 2.1: Confined structures with different dimensionalities.

confine one of their dimensions, we will obtain a nanoplatelet, which is considered as 2D (or quasi-2D) structure. Confining another dimension would result in 1D material, commonly known as nanowires or nanorods, and lastly confining quantum particles in all three dimensions would yield a quasi-OD structure widely known as quantum dots. An illustration of such confined structures can be seen in Figure 2.1.

2.3 Semiconductor Nanocrystals

Generally, materials are electrically classified as conductors, insulators and semiconductors. Semiconductors are materials of which electrical conductivity characteristics lie between those of conductors and insulators. The key factor which dictates a material's class is the position of the Fermi level. This level can be defined differently in different regimes but the simplest definition states that it is the highest occupied energy level by electrons at absolute zero temperature [32]. The location of this level in comparison to the energy bands defines the material's electrical conductivity. The Fermi level in conductors is located in an energy band that is partially occupied by electrons. This makes them extremely mobile in the presence of an external electric field and thus resulting in high electrical

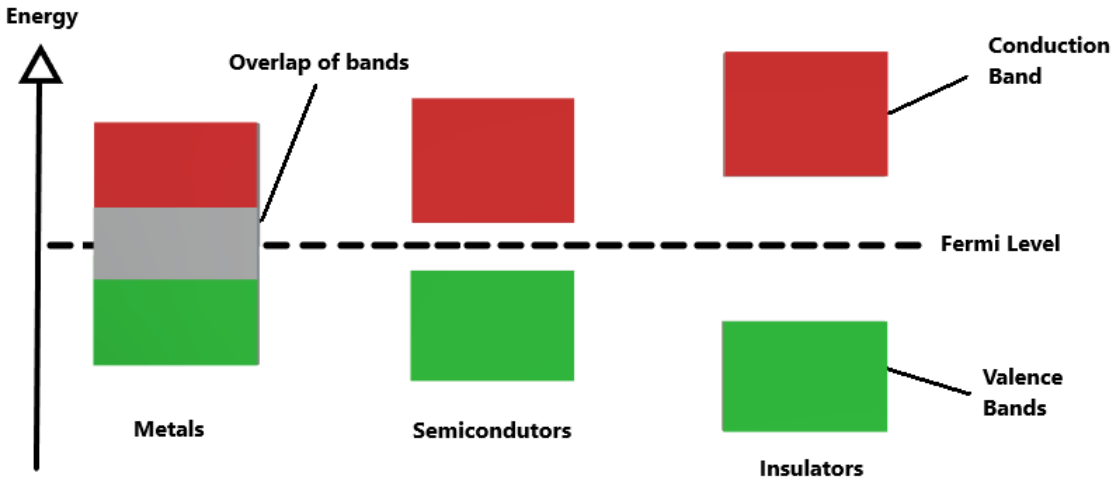

Figure 2.2: Bandgaps and Fermi levels of metals, semiconductors and insulators.

conductivity. In contrast, the Fermi level of insulators or semiconductors lies in some band gap, i.e., a region with no electronic state, and thus it is a forbidden region for electrons.

The energy bands are classified as conduction and valence bands. The conduction band is the closest energy state above the Fermi level, whereas the later one is the closest energy level below the Fermi level. At absolute zero temperature, the electronic energy states in insulators and semiconductors below the Fermi level are entirely filled, while those above it are fully unoccupied.

The width of a material's energy bandgap determines whether it is an insulator or a semiconductor. Materials having bandgaps of 3 eV or greater are categorized as insulators, whereas materials with smaller bandgaps are classified as semiconductors [33], [34]. Some common examples of semiconductors are silicon, Si, germanium, Ge; and similarly, glass, plastics, and wood are some common insulators.

A more detailed and in-depth picture of these bandgaps and electrical characteristics can be understood by the dispersion relations of the materials. The origin

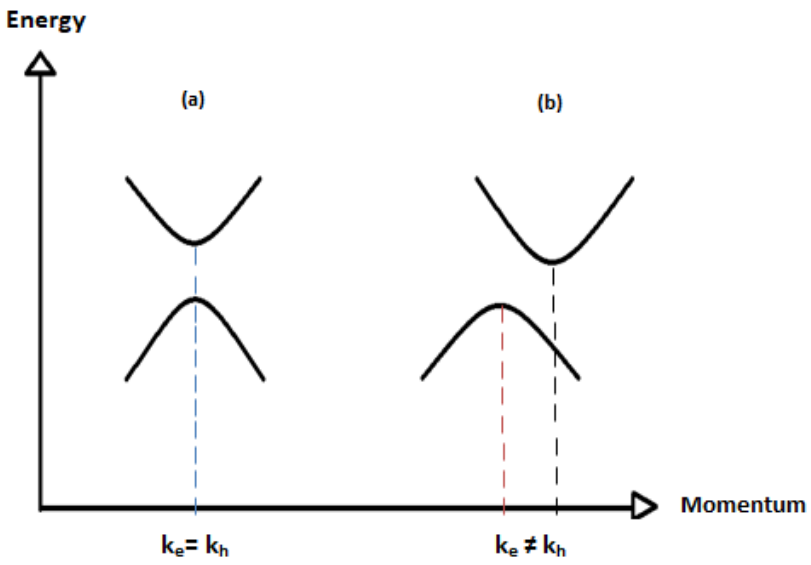

Figure 2.3: Characteristics of energy-momentum curves for semiconductors with (a) direct and (b) indirect bandgaps.

of the bandgaps arises from dispersion relations, which are energy-momentum *(E-k)* relations. The structure of these bands can be comprehended by solving the Schrödinger equation or density functional theory (DFT). Since the Schrödinger equation becomes quite complicated for systems with two or more than two electrons, so approximations along with DFT are usually employed to obtain E-k relations. In solid semiconductors, there is a certain pair of momentum and energy corresponding to an electronic state. Thus, it is more meaningful to talk about dispersion relations and have an idea about their origin.

There are two further classes of semiconductors from the bandgap's perspective: direct and indirect bandgap semiconductors. Direct bandgap semiconductors have the same k-value for electrons and holes in both the conduction and valence bands. In contrast, electrons in the conduction band and holes in the valence band have distinct k-values for indirect bandgap semiconductors. The illustration of these classes can be seen in Figure 2.3, where the momenta of electrons and holes are denoted as k_e and k_h, respectively.

Holes are quasiparticles created when an electron is excited by absorbing energy from the valence band to the conduction band or from a lower to a higher energy state, leaving behind a vacancy of an electron. Collectively, electron-hole pairs are known as excitons, and the de-excitation process of electrons from a higher energy band to a lower one is known as the recombination process. Now seeing Figure 2.3, it is clear that the maxima and minima of k-values (k_e and k_h) for direct bandgap semiconductors lie exactly on top of each other in the E-k curves. In contrast, the k_e and k_h values are not the same for indirect bandgap semiconductors. InP, CdSe, and ZnS are some common examples of direct bandgap semiconductors, whereas Ge and Si are in the list of indirect bandgap semiconductors.

In optoelectronics, direct bandgap semiconductors are of more importance since they provide photoluminescence. In photoluminescence, a photon is used to excite an electron from the valence band to the conduction band, making a vacancy of an electron in the valence band known as a hole. In absorption photoluminescence, the reciprocal process takes place: An electron in the conduction band and a hole in the valence band recombines, giving out a photon equal to the energy difference between the two bands. The electron and hole both make a contribution to electrical conductivity in their own way. The electron-hole pair, exciton, is a hydrogen-like quasi-particle attracted to each other by Columbic interaction. These quasi-particle have unique Bohr radius, which is the average distance between the electron and the hole, and effective mass. Later on, the recombination process releases a photon, if it is through a radiative process, or else it can be a nonradiative process, too. The process is illustrated in Figure 2.4.

An atom, in an isolated system, will have discrete and wider band gaps, whereas when a large number of atoms combine, the energy states come closer to each other and result in a continuum of energy states, known as energy bands. They are the result of a huge number of atoms in bulk materials, but as the number of atoms decreases, that is, sizes shrink like in NCs, the energy bands turn into discrete energy states. The number of atoms in NCs lies approximately between 100 to 10^5 [36]. Therefore, decreasing the size to these many number of atoms

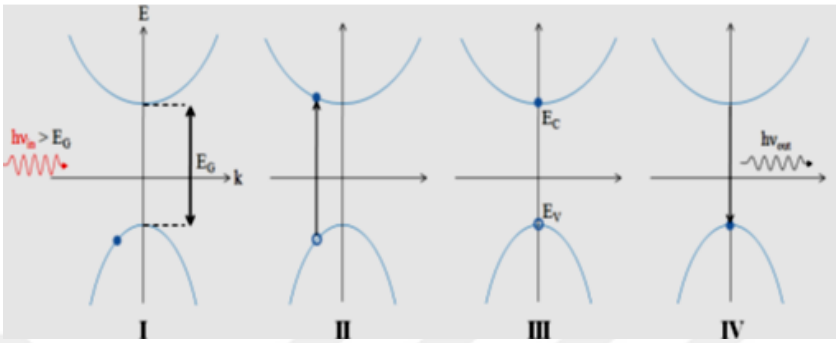

Figure 2.4: Photoluminescence process in semiconductors: (I) Excitation of an electron by absorbing a photon of bandgap energy, (II) a hole is created in the valence band due to excitation of the electron, (III) both particles, electron and hole, relaxes to the band edge, and (IV) recombination of electron and hole resulting in the emission of a photon [35].

and hence discretization of energy states changes the material properties [37]. Furthermore, the bandgap also changes drastically as the size of the material is altered. We may return to the problem of "particle in a box" where the well width modifies the structure of energy states, as can be seen from Equations 2.2 and 2.3. Since the discretization of states occurs in NCs, so they are also commonly referred to as artificial atoms.

Another way to understand the change in the structure of energy states is the confinement effect. In bulk materials, the electrons are free in to move in all three dimensions so the energy and momentum are related to each other with a relation

$$E = \frac{p^2}{2m} \tag{2.4}$$

which, for quantum particles, becomes

$$E = \frac{p^2}{2m} \quad and \quad since \quad p = \hbar k \quad so \quad E = \frac{\hbar^2 k^2}{2m} \tag{2.5}$$

There is no quantization in energy or momentum states in bulk materials. Considering again a simple example of "particle in a box" and its mathematical

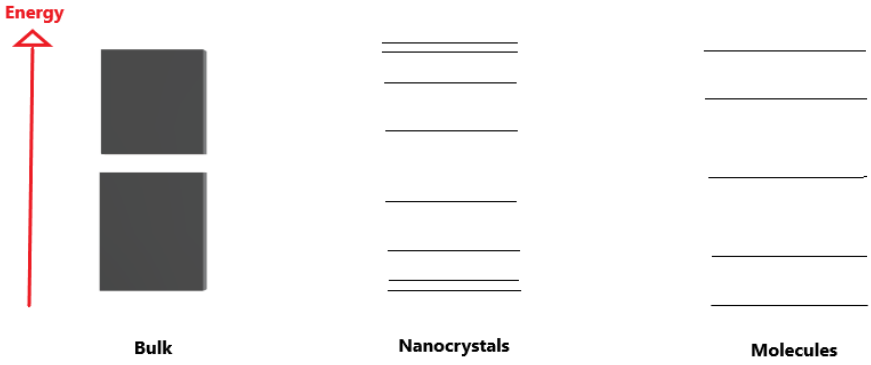

Figure 2.5: Distribution of energy levels in bulk materials, nanocrystals and molecules.

formulation, we can conclude how reducing size introduces quantization in energy and momentum. In quantum mechanics, we solve for all systems using the Schrödinger equation

$$\hat{E}\psi = E\psi \tag{2.6}$$

Here, "ψ" is the wave function, "$\hat{E}$" is the energy operator, and E is expressing total energy of the system, i.e., potential and kinetic, and in this system potential energy is zero, so the equation 2.6 becomes

$$-\frac{\hbar^2}{2m}\frac{d^2\psi(x)}{dx^2} = E\psi(x) \tag{2.7}$$

The general solution of Equation 2.7 gives us sinusoidal functions for ψ(x) and after using the boundary conditions for our system, i.e., for a particle being trapped in a box of length x=0 to x=L, we obtain quantized values for k:

$$k_n = \frac{n\pi}{L} \tag{2.8}$$

with a mathematical constraint on *"n"* only being able to take integer value and thus introducing quantization of states in momentum and also in energy too, if we insert back the value of k_n back in Equation 2.5. Now changing the values of L, either shorter or wider, changes the structure of energy states in the system. Using the reference of particle in a box is just for developing some basic understanding about the impact of size on energy states, but one should not forget

that the real systems are way complex and hard to solve.

The confinement energy of quantum systems directly depends on sizes. For example, for quantum dots, the energy is dependent on the diameter of the confinement [38].In a similar fashion, the exciton energy also increases if it is in a confined particle rather than in bulk. A theoretical calculation of this enhancement of excitonic energy is available in the literature for quantum wells [39] and for some of the spherical NCs [40]. The increase in energy is often more noticeable when the size of the structures approaches the size of the exciton Bohr radius. In the 1980s, the prediction of quantum size effect was first observed for semiconductor nanocrystals grown in glass matrices [41], [42]. Murray *et al.* described a low-cost reproducible colloidal synthesis process based on nucleation for several Cd-based NCs such as CdTe, CdS, and CdSe, which sparked a surge in nanocrystal research. Murray *et al.* showed the production of highly monodisperse, with a size dispersity of 5% spherical NCs through their synthetic approach, with NCs ranging from 2 to 11nm in the ensemble. Along with that, Murray *et al.* demonstrated the tunability of the absorption spectra of their synthesized NCs by varying their sizes. For an example, a transmission electron microscopy (TEM) image of core/shell CdSe/ZnS QDs is shown in Figure 2.6, synthesized by Demir's group.

The TEM micrograph illustrates crystallographic planes of these QDs (synthesized by our group) that are quite visible. These nanocrystals are usually stable and therefore, dispersed in nonpolar organic solvents. The dispersion of these nanocrystals is assisted by the surface passivation of organic ligands like oleylamine and oleic acid in the organic solvents. The dispersion of NCs is not only limited to organic solvents, but there is some evidence in literature where researchers have dispersed these nanoparticles in polar solvents, too [43] with some alternative synthesis routes and different surface ligands have been used. Ligand exchange procedures can be used as an alternative where the native ligands are replaced with distinct ones [44]. The process of ligand exchange is quite common to vary the activity or function of their NCs. This is used for better solubility of NCs in a certain solvent such that the size of NCs remains unchanged for later uses

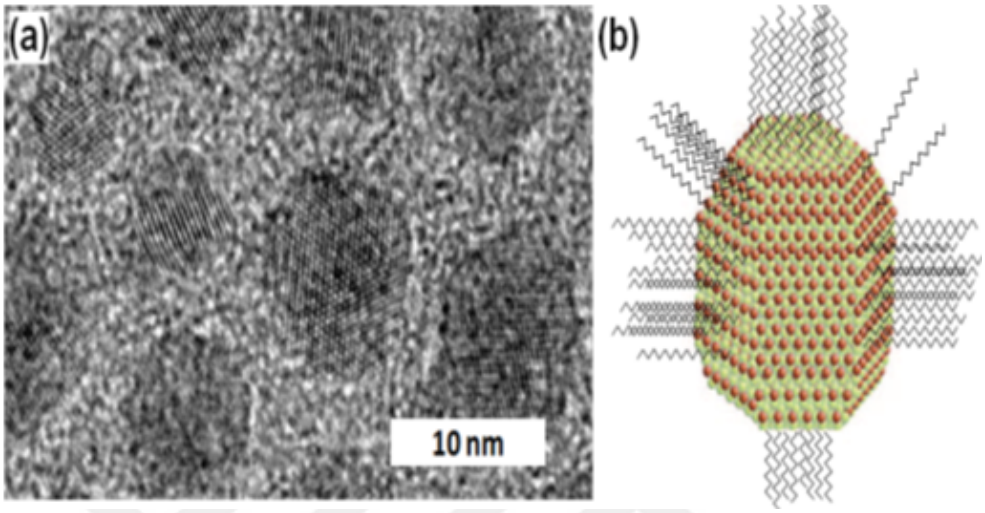

Figure 2.6: (a) A TEM micrograph of CdSe/ZnS core/shell QDs synthesized by Demir's group, and (b) a schema of quasi-spherical shaped QD along with ligands attached on the faces of QD. Adapted with permission from Ref. [36] Copyright 2023 American Chemical Society.

and the NCs do not agglomerate. Sometimes ligand exchange is also employed to enhance device functionalities. For example, to obtain electroluminiscence, as an active media, in optoelectronic devices, one might use some shorter-length ligands to enhance the charge transportation and hence the device performance. Moreover, ligands also take care of the dangling bonds. These are present on the surface as the periodicity of the crystal structure is broken down on the surface, so the atoms here rearrange themselves and therefore, some are left unsaturated, thus making these sites highly energetic and causing surface traps for charges. Such trapping mechanisms are not desired in optoelectronic devices as they create nonradiative recombination channels and reduce the photoluminescence (PL) of the NCs and in turn, the efficiencies.

The deposition of a shell around and onto the core is also used as surface passivation of the core NCs. These shells must be lattice compatible to protect the structural and optical characteristics of the cores. This coating can be achieved colloidally and results in improved stability and quantum yields of the NCs. This modifies the bandgap, which results in red-shifted absorption and PL spectra

of the material. Therefore, different semiconductor NCs, according to the need, can be synthesized in different shapes and compositions to be utilized for various applications such as solar cells [45], [46], LEDs [47] lasers [48], [49].

To date, several classes of NCs, including spherical QDs, nanocubes [50] nanorods [51], and nanoplatelets [52], [53] have been synthesized. We will talk in detail about an emerging class of quasi-two-dimensional semiconductor NCs of nanoplatelets (NPLs) or colloidal quantum wells (CQWs).

2.4 Colloidal Quantum Particles

In this chapter, we will talk more precisely about the NPLs and CQDs on which we have worked in this research tenure.

2.4.1 Colloidal Quantum Wells (CQWs or Nanoplatelets NPLs)

A more recent two-dimensional class of NCs is known as CQWs. CQWs, or interchangeably the NPLs, are quasi-two-dimensional structures with one confined dimension, suppose z-direction. These platelets have lateral dimensions in tens of nanometers, whereas the vertical thickness is a few nanometers. Their confinement is only apparent along the vertical dimensions as long as the lateral dimensions of these CQWs are relatively larger than the Bohr radius, and thus electron and hole can be considered to have free motion in the lateral dimensions. It can be seen that the energy of a particle in such a quantum box through the equation as

$$E_n = \frac{n^2\pi^2\hbar^2}{2mL^2} + \frac{\hbar^2 k_x^2}{2m} + \frac{\hbar^2 k_y^2}{2m} \tag{2.9}$$

and this is known as confinement energy.

One of the exciting properties of these platelets is their atomically flat surface.

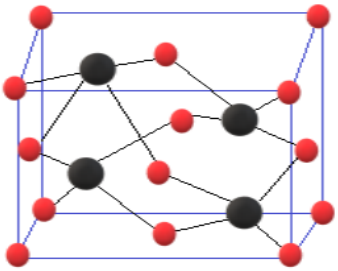

Figure 2.7: Schematic of cubic zinc blende structure of CdSe crystals (red sphere: Cd atoms, black sphere: Se atoms).

This results in the reduction of inhomogeneous emission broadening due to size dispersion, and their emission linewidth is several nanometers [9] at room temperature, making them superior to QDs in this manner.
Ithurria *et al.* first synthesized reproducibly different zinc-blende structures of CdSe CQWs. The structural changes were in the vertical thickness, which ranged from 3.5 to 5.5 monolayers. These monolayers (MLs) represent the alternating layers of Cd and Se atoms in the CdSe. For example, 1 monolayer means a thickness of two planar separations between Cd-Se-Cd atoms, i.e., around 0.148 nm x 2 = 0.296 nm, calculated using Figure 2.7, and similarly, 4.5 ML means that this structure has a thickness of around 1.3 nm. This precision is allowing the thickness control at the atomic level [8]. Figure 2.7 shows a schematic of the cubic CdSe structure.

The thickness calculation is carried out using the bond length, as 2.61A [54], along with geometrical analysis, yielding a thickness of around 1.2 nm for 4.5 ML CdSe, resulting in a shorter dimension than the excitonic Bohr radius of CdSe CQW, which is 5.4 nm [55]. Figure 2.9(a) shows the TEM image of CdSe CQWs 4.5 ML thick, along with their schematic and figure 2.9(b) shows PL and absorbance spectra of 3.5, 4.5, and 5.5 ML CQWs. The difference in the peaks exists because

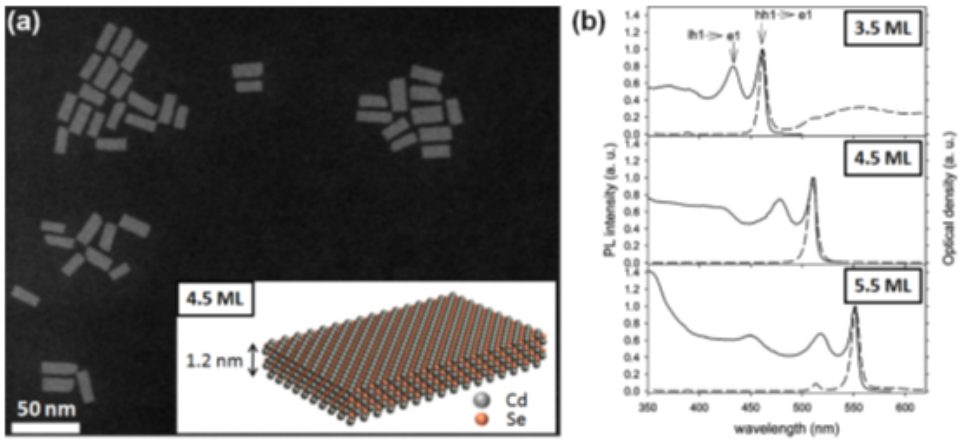

Figure 2.8: (a) TEM image showing the top surfaces of 4.5 ML CdSe CQWs along with their schematic, with a vertical thickness of 1.2nm (b) shows PL and absorption spectra of 3.5, 4.5, and 5.5 ML of CdSe CQWs. Adapted with permission from ref. [11]. Copyright 2023 American Chemical Society.

of different thicknesses of the CQWs and hence different confinement extents.

As seen in Figure 2.8b, different PL peaks represent different colors of emitted light, which is possible by adding 1 ML to the CQWs and hence inducing discretization in PL tunability. In contrast, spherical CQDs have continuous spectral tunability by just adjusting their radii. So in this manner, one can consider CQDs as superior than CQWs. Nevertheless, the colors from CQWs can be tuned alternatively by adding different compositions of alloys [56] or by depositing layers of shells onto the cores [57], [58].

Different group elements in the periodic table have been studied, to date, for the synthesis of CQW structures including ZnS, PbS, HgTe and their doped CQW structures [59]. At the moment, high purity techniques for the synthesis of II-VI semiconductor CQWs materials are limited and CdSe is among the most commonly synthesized II-VI semiconductor CQWs. The cadmium-based CQWs have been used in luminescence solar concentrators (LSCs) [60] exploiting the structural and intrinsic properties such as large absorption cross-section, arising due

to their structure, high quantum efficiencies and tunable dopant PL. Along with these, they already found their use in lighting devices such as LEDs [6], [61] and lasing [62]. Furthermore, they have intrinsic structural anisotropy, which results in planar emission from these CQWs [13]. This unique property can be utilized in lighting devices, either LEDs or lasers, for directional emissions if they are assembled in films with controlled orientations. To exploit this aspect, one must have an orientation-controlled assembly control of these CQWs to enhance device performances, and different techniques have been used to achieve a controlled assembly of the NCs, which will be discussed in the next chapters.

2.4.2 Colloidal Quantum Dots (CQDs)

Development in electronics has always eyed low-cost and solution-processed semiconductor materials because of their significant advantages. Quantum dots, abbreviated as QDs, are the main class of semiconductor nanocrystals with size and bandgap tunability. These structures are confined in all three dimensions and are commonly known as 0D materials. The diameter of CQDs usually lie below 20 nm [63], depending upon the excitonic Bohr radius of the material. To be in the strong or moderate confinement regimes, the dimensions must be smaller than or equivalent to the excitonic Bohr radius of the material. The confinement energy for a particle with mass *'m'* in such a dot is given as

$$E_{n_{x,y,z}} = \frac{\pi^2\hbar^2}{2m}\left(\frac{n_x^2}{L_x^2} + \frac{n_y^2}{L_y^2} + \frac{n_z^2}{L_z^2}\right) \tag{2.10}$$

L_x=L_y= L_z to approximate a spherical or form a cubic QD. Therefore the above equation changes to

$$E_{n_{x,y,z}} = \frac{\pi^2\hbar^2}{2mL^2}(n_x^2 + n_y^2 + \{n_z^2) \tag{2.11}$$

with *'L'* being the side length of a cube (if it is a cubic QD) or the diameter (in the case of spherical QD). A schematic of such QDs is shown in Figure 2.9.

Both shaped QDs have different significance and can be utilized in the devices accordingly. These QDs can be obtained using either of the common techniques:

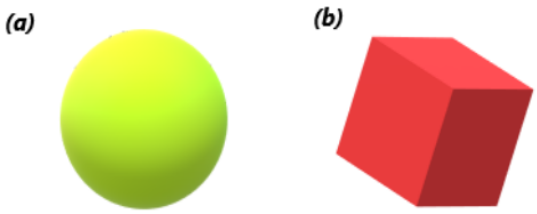

Figure 2.9: Schematics of (a) spherical QD and (b) cubic QD.

epitaxially grown or colloidally synthesized. Colloidal quantum dots can be synthesized from the elements of groups II-VI, I-III, III-V and IV-VI since their first discovery in the 1980s [64]. They are commonly used in photonic devices such as LEDs [65], lasers [66], and also in solar cells [67] and photodetectors [68].

Techniques for wet chemical synthesis, such as hot injection [63] procedures, are used to synthesize CQDs. The size control over these CQDs is achieved by the selection of precursors, concentration of precursors, reaction time and temperature during its synthesis [1]. Once the size is in the order of Bohr radius, discretization of states takes place, allowing for bandgap tunability and thus emission and absorption spectral tunability, covering a wide range of spectrum from UV to visible to IR. Apart from the size and shape, the surfaces of the CQDs play a very important role in their electronic structure [69] and, therefore, in optoelectronic device performances and efficiencies when employed. The surfaces of CQDs are passivated with ligand molecules which make them stable in a solution phase, prevent from aggregation and make them non-interacting with each other. But these molecules affect the device performance since charge carriers form a barrier while transportation. Usually, native ligands are exchanged with some other ligands, e.g., nonconductive ligands replaced by conductive ones or longer ligands replaced by shorter ones, to enhance the performances.

CQDs can be utilized in the solution phase to form thin layers, as gain media of photonic devices, using spin-coating, spray-coating or self-assembly methods. Again uniformity, in terms of their assembly, plays an important role in avoiding unnecessary drops in device efficiencies. In the next chapters, we shall see the liquid-liquid interface self-assembly technique used to form active layers of the working devices.

2.5 Self-Assembly of Colloidal Semiconductor Nanocrystals

In simple words, self-assembly is the procedure or technique by which individual building blocks arrange themselves, given a favorable or preferred environment, to form ordered structures and superstructures [70]. This term is also used for the crystallization of atomic solids but in this thesis, we are reserving it for the arrangement of synthesized nanocrystals which are connected together via weak forces like van der Waals, hydrogen bonding or hard-particle interactions [71]. These nanocrystals can be self-assembled using external forces such as fluid flow and electric or magnetic fields.

A sample of synthesized nanocrystals can be stimulated to self-assemble to form an ordered superstructure by many ways, for example, evaporation of the solvent having nanocrystals, gravitational sedimentation or solvent destabilization [72]. From a practical perspective, self-assembly techniques provide a comparatively smoother, easier and low-cost bottom-up approach to produce complex 3D structures and material designs compared to top-down techniques unlike electron beam lithography or dip-pen nanolithography [70]. However, one must take into account the challenges encountered in the bottom-up techniques, especially for designing. Having nanocrystals with precise compositions, uniform shape and size, and surfaces often require synthetic expertise. Furthermore, employing self-assembly on these nanocrystals requires definite control of the environment, such as carrier solvent, substrate selection and temperature, etc., to obtain a desired

structure. Additionally, the formation of superstructures may also encounter undesirable formations in the structure due to the presence of polymorphs, which sometimes are hard to control during synthesis.

There are some common factors that drive the assembly process and they can be extensively complicated, especially for nanomaterials. Assemblies can be driven because of dipole-dipole interaction between nanocrystals. For example, CdSe nanocrystals can exist in zinc-blende or in wurtzite structures. The wurtzite structure of CdSe nanocrystal has a dipole along c-axis [73] from theoretical calculations. This can serve as a reason for the self-assembly process to be driven. Another possible reason behind the self-assembly process is the van der Waals force, whose origin lies behind the induced dipole-dipole interaction present in every material. If a material has no net time-averaged dipole moments, yet an instantaneous dipole exists because of the constant movements of electrons around the nucleus [74]. This instantaneous dipole will create an electric field in the vicinity, creating a net attractive force between two semiconducting nanocrystals. This inter-nanocrystal interaction, through a solvent, is generally given by Hamaker pair-potential as

$$V_{ij} = -\frac{A}{\pi^2} \int_{V_i} \int_{V_j} \frac{1}{r^6} dr_i dr_j \tag{2.12}$$

Here A is the Hamaker constant, and V_i and V_j are the volumes of the particles. This potential depends directly on the Hamaker constant, the separation between the particles and the geometry. Hamaker constant is calculated as A_{121}, meaning that constant of the material (1) through the solvent (2). The Hamaker constant for CdSe nanocrystals is calculated as $A_{CdSe} = 3.8 \times 10^{-20} J$ taken from ref. [75], yielding A_{121} in apolar solvent (like hexane), $A_{121} = 1.87 \times 10^{-20} J$, taken from ref. [76].

Similarly, self-assembly can also be driven through depletion interactions or forces. In this scenario, consider a solution of colloids along with smaller polymer chains; when large colloids approach each other, the small polymers are excluded from the space between two approaching colloids and thus allowing them to be attracted to each other through depletion. The reason why small polymers are excluded

from the space is conformational entropy.

To sum up, self-assembly is driven by either interaction of the functional groups, i.e., ligands [77] or through intermolecular interactions [78]. It is indeed not easy to grasp a full picture of the extent of factors driving the self-assembly phenomenon but one can surely make use of these factors to create a favorable environment for the nanoparticles to self-assemble. In later chapters, we shall see some commonly employed self-assembly techniques for our semiconductor nanocrystals.

Chapter 3

Materials and Methods

3.1 Synthesis

Semiconductor NCs can be prepared using well-known techniques such as epitaxial growth and colloidal synthesis. In Table 3.1, we can see some examples of these techniques commonly employed for synthesizing nanomaterials. All of the techniques mentioned in the table have their own advantages and are used for certain purposes. Here, we will talk only about colloidal synthesis techniques employed to synthesize NCs, specifically 4 ML CdSe and its heterostructure.

The liquid phase synthesis method, such as colloidal synthesis, has emerged as an excellent tool for synthesizing NCs as it offers a broad range of size and shape control [79]. In this synthesis method, a precursor comprising an organometallic compound or inorganic salt is reacted in the presence of stabilizing agent in a liquid medium. The precursor ultimately frees the monomers responsible for the nucleation and growth of NCs [80]. In general, the steps for a colloidal synthesis route are (i) nucleation, i.e., when a required concentration of monomers is reached in the mixture (ii) growth, i.e., when the formed nuclei grow larger than converting back into monomers, and lastly (iii) stop the growth, i.e., quenching process.

Nanomaterial synthesis techniques		
Physical techniques		**Chemical techniques**
Mechanical-techniques Mechanical milling	**Vapor techniques** Physical vapor deposition (PVD) • Sputtering • Laser ablation • Laser pyrolysis	• Sol-gel • Chemical vapor deposition (CVD) • Colloidal method • Spray pyrolysis

Table 3.1: Different synthesis techniques for nanomaterials.

The advantages of colloidal methods are that they are the easiest and cheapest way to create nanoparticles. Furthermore, this technique allows us to use both organic and inorganic reactants, enhancing the range to synthesize nanoparticles. Additionally, this technique can be used for the mass production of NCs [80].

3.1.1 Cadmium myristate

To synthesize core CdSe, we need cadmium myristate (Cd(myr.)), $C_{28}H_{54}CdO_4$ and a white color powder. In the literature, cadmium myristate was prepared according to the recipe [81] with slight modifications. Sodium myristate (3.13 g) in methanol (250 mL) was added to the reagent bottle. Another reagent bottle was prepared with 1.23 g of cadmium nitrate in 40 mL of methanol. Both the reagent bottles were left for continuous stirring for a duration of 2 h and the solids were dissolved. After that, both solutions were mixed in a single reagent bottle and left for another span of continuous stirring for 2 h. Using a centrifuge, a white powder of Cd-myr was precipitated out. The cadmium myristate was then rewashed twice to remove impurities with methanol. Finally, the precipitate was left in the desiccator under vacuum and at room temperature for 24 h to dry it.

3.1.2 4 ML CdSe Core CQWs

We can now start synthesizing the material mostly employed throughout this thesis research: four monolayer cadmium selenide cores (4 mL-CdSe). In the beginning, we need to weigh 340 mg of Cd-myr and 24 mg of selenium (Se), and then add both of these powders in a 3-neck synthesis flask along with 30 mL ODE, measured using a measuring cylinder, and left for degassing at 90^0C for 1 h. We then need to turn on the gas, argon, and increase the temperature to 240^0C. When the temperature reading goes around 192^0C, we add 120 mg of cadmium acetate diydrate. At this point, the color of the mixture turns orangish. The mixture is under constant stirring, and by the time we add cadmium acetate dihydrate, we start the stopwatch and give the mixture 8 min as growth time. Last, the growth is terminated by the addition of 1 mL of oleic acid (OA), and the solution is quenched in a water bath. The solution was centrifuged at 6,000 rpm for 6 min, then ethanol was added to the supernatant until the color turned milky, and then centrifuged again for 6 min at 6,000 rpm. Finally, the precipitate was dispersed in hexane, and the solution was sonicated and kept for further use.

3.1.3 4 ML Core/Shell CdSe/CdZnS CQWs

Shells are coated on cores for many reasons, such as to enhance photoluminescence quantum yield (PLQY) or to cover a broader range of spectra. Here we start by measuring a volume, corresponding to 4 optical density, of already synthesized 4 ML cores and adding them to 22 mg of anhydrous Cd-Acetate, 73 mg of anhydrous Zn-Acetate, 7 mL ODE, and 1 mL of OA. All of these are added to a 3-neck synthesis flask of 50 mL and left for degassing for an hour at room temperature. The temperature is increased to 85^0C, in small increments, and left for further degassing for around 30 min. Then, we need to turn on the gas, add 1 mL of oleylamine (OLA), and the temperature is increased to 300^0C. At around 160^0C, we start the injection of S-precursor (5 mL) prepared by making a mixture of 8 mL ODE and 140 μL of octanethiol. In the beginning, the injection rate is set to 10 mL/h, and then it is decreased to 4 mL/h when the temperature is 240^0C. We

then wait for the injection to complete, and as soon as the desired PL is reached, we stop the injection and then quench it. Last, the NPLs are washed using the same protocol as for the cores and then dispersed in organic solvent, e.g., hexane and toluene.

3.1.4 Ligand Exchange

The common ligands deployed on the facets of CQWs are OLA and OA. Here we replace them with shorter ligands which enhance device performance by reducing the path for the charge carriers when used in devices. Under the gas flow, 150 μL of 2-ethylhexane-1-thiol (EHT) is added to the flask containing 1 mL of NPLs solution with an optimized concentration of 100 mg/mL while stirring. The solution is left under the argon environment for stirring for 2 h giving enough time for ligands to replace the previous ones. The NPLs are then precipitated by adding ethanol and then re-dispersing in the organic solvent. The process is repeated two times, but this time the amount of EHT added to the same amount of NPLs is 50 μL. At last, the NPLs were washed with ethanol and re-dispersed in hexane. A picture of the synthesis line used in the lab is shown in Figure 3.1.

3.2 Self-Assembly Techniques for Nanocrystals

In the previous chapter, we have seen what drives the self-assembly process at the atomic scale, and also the significance of the SA of nanocrystals. In this chapter, we will see different techniques in the literature, usually employed for the self-assembly of nanocrystals, the macroscopic reasons behind the SA process, and the advantages or disadvantages of the techniques.

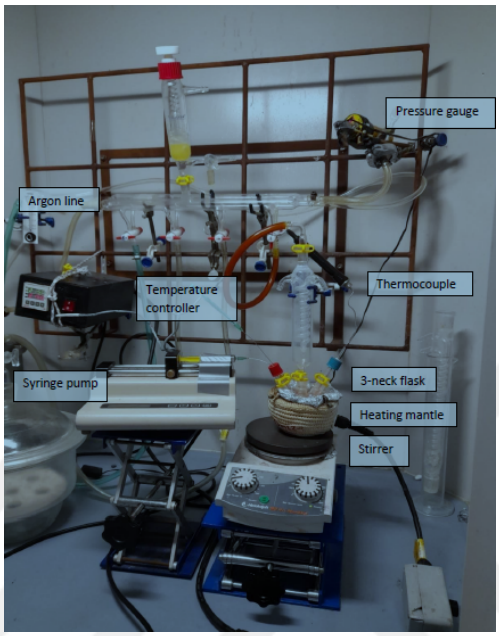

Figure 3.1: Schlenk line used for all the synthesis in this thesis at Demir's lab.

3.2.1 Solvent Destabilization

To achieve 3D superstructures from nanocrystals, this technique has been used in the literature [70]. In this case, adding a non-solvent in the solution of nanocrystals induces attractive interactions between dispersed NCs and leads to their self-assembly. The colloidal systems remain stable as long as there is no aggregation of NCs due to the presence of counteracting force to Van der Waal's force. This counteracting force is coming from the ligands which enhance colloidal stability and therefore, the addition of an anti-solvent reduces this barrier and gives rise to the NCs aggregation [1]. This type of SA technique does not usually form thin layered structures but rather 3D structures like polyhedra or spherical. This approach has been employed to self-assemble nanocrystals like nanorods [82] and platelets [83]. The schematic of the process is shown in Figure 3.2.

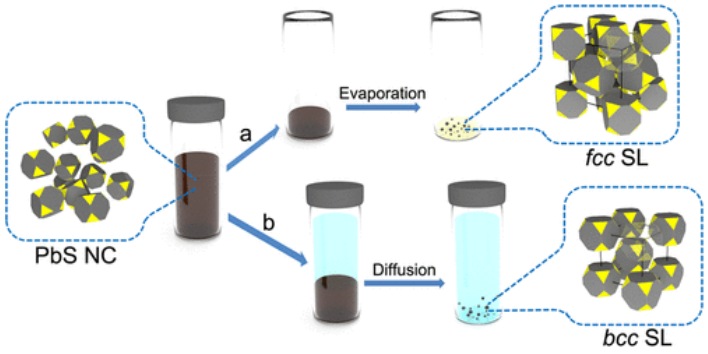

Figure 3.2: Slow diffusion of solvent and anti-solvent into each other in a sealed veil, resulting in the self-assembly of PbS NC through solvent destabilization. Adapted with permission from [84] Copyright 2023 American Chemical Society.

3.2.2 Drop-Casting

This method is very simple and exploits the evaporation of the solvent of NCs solution to achieve the SA layer. Herein, a small volume of dilute NCs solution is dropped on a solid substrate and allowed to evaporate for some time (usually several minutes). For organic capped ligands, a solvent with a mixture of hexane and octane in a ratio of 9:1 (by volume) yields ordered superlattice [85]. The assembly is driven because the particles are trapped at the interface of liquid and air, forming 2D membranes [86]. A real-time evaporation-based assembly can be seen in Figure 3.3.

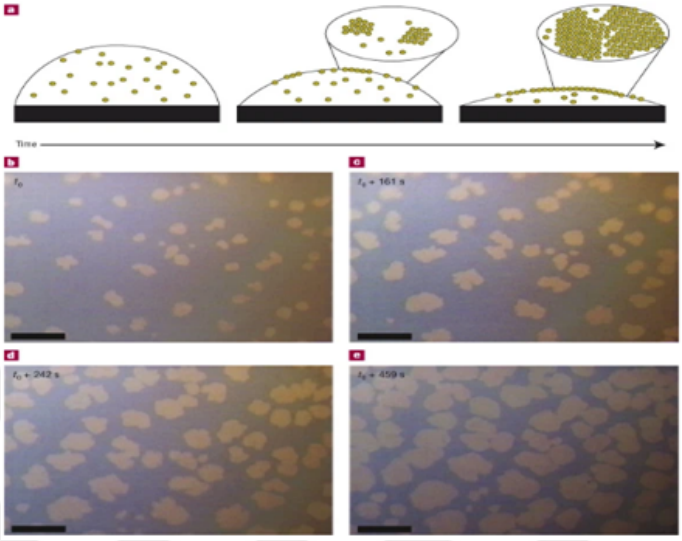

Figure 3.3: The NCs are gold NCs with ligands dodecanethiol. (a) Schematic of the drop-casting process and (b)-(e) real-time optical microscopy images showing island formation due to solvent evaporation as time passes. Adapted with permission from [86] Copyright 2023 Springer Nature Limited.

3.2.3 Langmuir-Blodgett Method

The evaporation-based techniques are not limited to solid substrates; the idea can also be extended to liquid subphases as well. Herein, a drop of NCs solution is dropped on a liquid that is not miscible with the solvent of NCs solution. The film is then compressed using barriers until they form a monolayer of NCs after the evaporation of the solvent. Lastly, the already submerged substrate is lifted vertically with a constant speed while the barriers keep compressing the film to maintain the monolayer of the NCs. Each lift-off of the substrate or immersion puts an additional layer of NCs. The process is illustrated in Figure 3.4 for QDs with organic ligands.

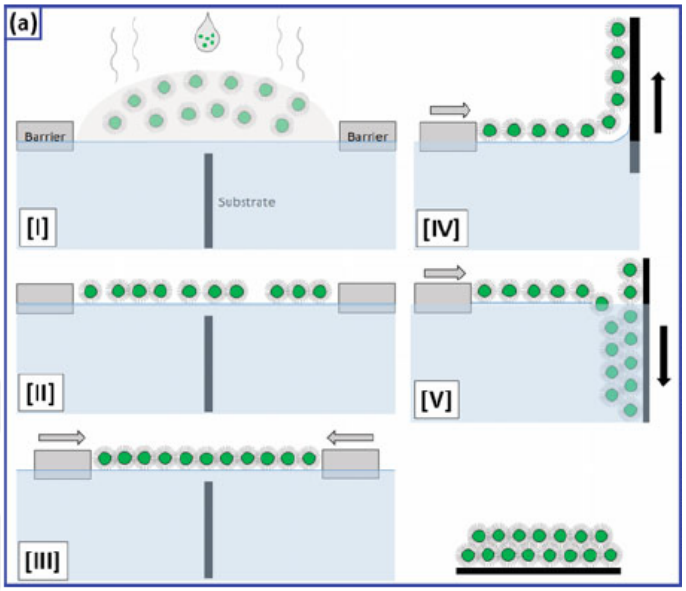

Figure 3.4: An illustration of Langmuir Blodgett self-assembly method, taken from [87].

3.2.4 Liquid-Interface Self-Assembly

In this section, we will talk about the self-assembly method used to assemble the particles in this thesis. Herein, we have employed an assembly technique similar to the LB method but not exactly the same. We have performed the SA of NCs on two immiscible liquids through a controlled evaporation of the solvent directing the assembly. Before digging further into it, the term solvent is specifically used for the nonpolar solvent in which NCs are dispersed, whereas the term subphase is used for the polar solvent over which NC solution is spread.
The schematic of liquid-liquid or simply liquid interface self-assembly can be seen in Figure 3.5. Herein, a solution with optimized concentration and volume of NCs in a non-polar solvent is spread over a polar solvent to obtain a layer of assembled NCs. As the solvent evaporates, in a controlled fashion, the subphase is pulled out, and therefore, part of the film is deposited onto the substrates.

This SA technique is used to assemble Fe_3O_4 NCs dispersed in hexane and dropped over acetonitrile or ethylene glycol (used as a polar subphase) in the

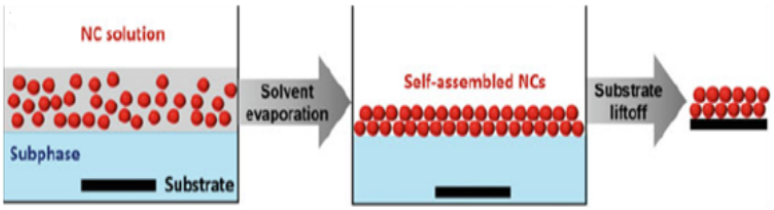

Figure 3.5: Schematic of self-assembly method, taking place at the interface of two immiscible liquids, known as liquid-interface self-assembly [35].

literature [88]. In another report, CdSe NPLs were self-assembled with orientation control using the same technique [24]. The method also allows for large-area deposition of the NCs, with an example of the self-assembly of Fe_3O_4 and FePt nanocrystals in the literature [89].

The technique has enhanced its benefits further since it allows orientation control of the anisotropic NCs, which is an important tool for studying film characteristics with certain orientations of NCs. In addition to NPLs, researchers have employed this method to control the orientation of nanorods (NRs) as well [90]. Apart from evaporation rate control to dictate the orientation of anisotropic NCs, scientists have used other methods, too, such as adding additives to alter the interaction potentials of inter NCs and NCs-subphase [13], where Gao *et al.* controlled the orientation of CdSe NPLs by adding oleic acid in a concentration-dependent manner. However, such techniques achieve orientation control at the cost of losing the purity of films, which directly affects device performance.

So herein, we have used this method to control the assemblies kinetically through the evaporation rate control of the solvent and the selection of subphases. This has allowed us to sustain film quality as this does not require additives to be added to control orientations of NCs. In short, we have achieved pure and well-oriented films of anisotropic nanoparticles by adjusting macroscopic entities. Nevertheless, one must not forget the impact of minor factors acting on the quality of

self-assembled films such as concentration and dropping amount, thus, these factors must not be ignored. We will see the detailed results in the next chapters.

Chapter 4

Results and Discussions

As this thesis work is related to the self-assembly of nanocrystals using the liquid interface technique, this chapter will cover the results for two different classes of nanocrystals: CQWs and CQDs, for which we systematically carried out the self-assembly for a variety of device applications.

4.1 Colloidal Quantum Wells

The most important and thoroughly studied self-assembly, in this thesis, is for CdSe CQWs and their heterostructure (core/shell). Majorly, examples included the self-assembled cores CdSe and core/shell CdSe/CdZnS with organic oleic acid ligands.

4.1.1 4-Monolayer CdSe CQW Cores

It has been already discussed in the previous chapters about the material, and synthesis. Here we present the optical characteristics including PL and absorption spectra of the material and SEM results of their self-assembled layers.

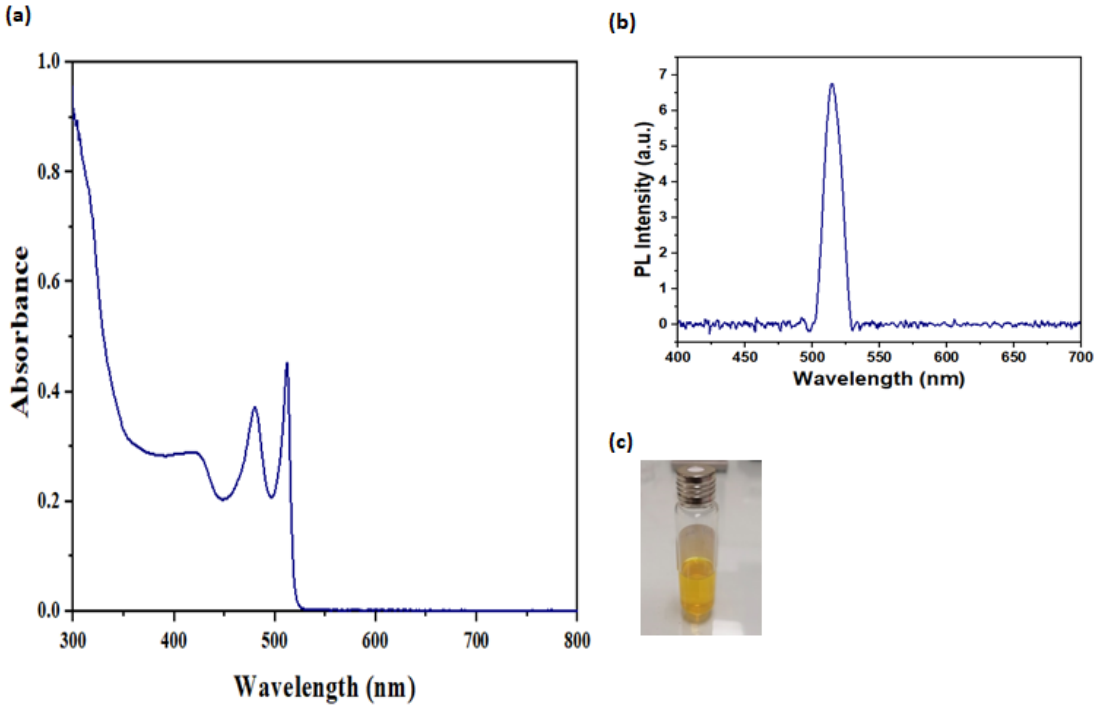

Figure 4.1: (a) Absorption spectrum and (b) PL spectrum where a 400 nm laser was used to excite, and (c) photograph of the sample emitting at $\sim$ 510 nm.

The optical properties of 4 ML core SdSe CQWs are shown in Figure 4.1.

The self-assembly was then performed using the liquid interface technique, where whole films of NPLs were deposited, with all NPLs either in facedown or edgeup orientation.

To prepare the facedown (FD) film, first NPLs were washed three times by adding ethanol and then centrifuged. The supernatant was disposed off, and NPLs were re-dispersed in hexane. The amount of hexane was added carefully to reach the desired concentration. Finally, NPLs were prepared with a concentration of 25 mg/mL. The liquid subphase used in this case was acetonitrile (ACN), teflon container used was a circular one with a diameter of 8 cm.

To deposit the films and analyze the assembly, two types of substrates were used:

Figure 4.2: Instruments, tools, and materials used to carry out liquid-interface self-assembly.

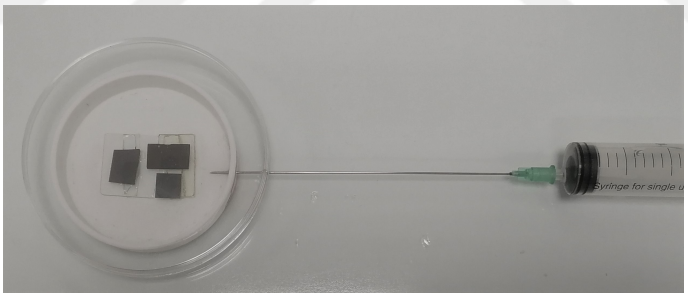

Figure 4.3: Our home-built setup for self-assembly.

either quartz or silicon substrates with a size of 1 cm^2. To wash the substrates, they were put in a beaker and first of all 100 mL of DI water was added along with 100 μL of Hellmanex. The solution was sonicated for ∼10 min. Subsequently, it was disposed of and cleaned with DI water and sonicated for ∼10 min. Then, the substrates were washed with acetone and sonicated for again 10 min. Last, they were washed with isopropanol along with 10 min of sonication. The substrates were then dried and kept in a petri dish for later use.

To describe the SA process, the instruments, and setup are shown in Figures 4.2 and 4.3, respectively.

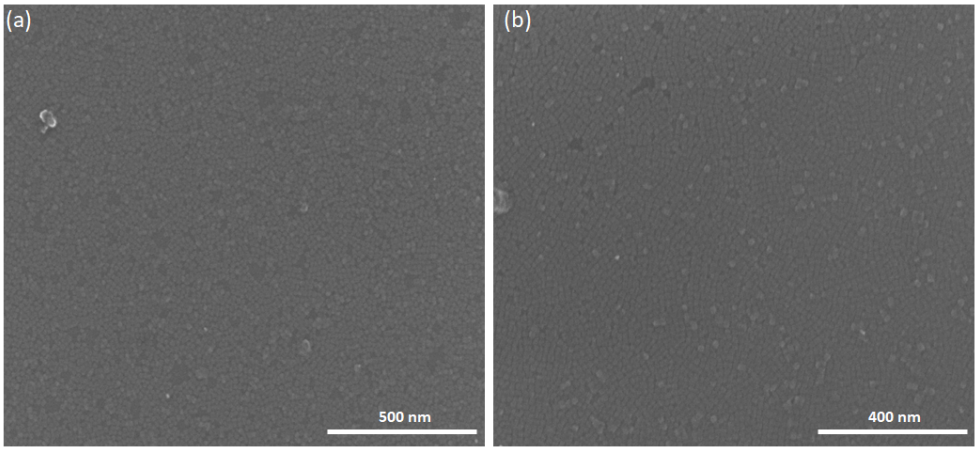

Figure 4.4: Facedown orientation of 4ML CdSe core NPLs on dummy Si-substrate, taken using immersion mode of FIB's SEM gun, with (a) and (b) at different magnification scales.

Once the setup is ready, we proceed with the self-assembly process. First of all, we added the subphase in the Teflon well as shown in Figure 4.3, then we dropped 10 μL of the optimized solution of NPLs on a side wall of the Teflon and cover it with a lid. We then checked with a laser to see uniform spread of NPLs on top of the subphase. This concentration and dropping amount covered the whole Teflon area and we found these optimized numbers by error and trial method. After covering the lid, we waited for ∼3-5 min and then pulled the subphase using a syringe. Last, the samples were kept in the desiccator for controlled drying. So, the single layer film of 4 ML square cores all in facedown orientation was prepared and can be seen in Figure 4.4. With this method, one can deposit a facedown layer of NPLs up to several tens of centimeters, limited by teflon's dimensions.

The experiments were repeated several times to check the reproducibility and consistency. We then deployed this technique for the deposition of the active layer of photodetectors. Photodetectors are optoelectronic devices that convert an optical signal to an electrical signal in general. The purpose of employing self-assembled layers of CdSe NPLs was to study the impact of oriented self-assembly on the response time of the device, i.e., time required by charge carriers to reach the electrodes. In a random orientation of NPLs, charge carriers would require

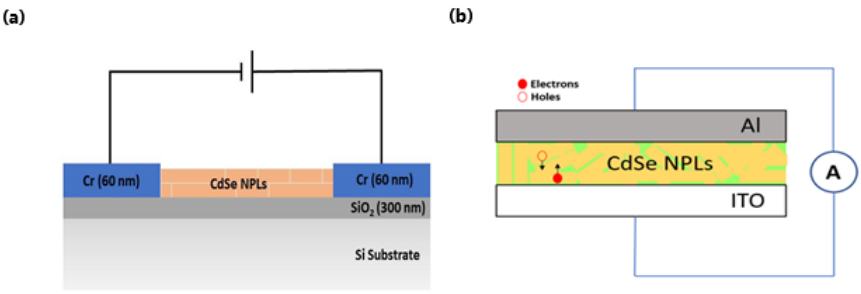

Figure 4.5: (a) A lateral photodetector and (b) a vertical configuration of the photodetector.

more time to reach the electrodes. On the other hand, if all NPLs would be in a specific orientation, the time required to cover the distance to electrodes would be shorter since the effective distance would be much shorter, too. Nevertheless, this thesis work was restricted to depositing a uniform layer of self-assembled layer of NPLs with controlled orientation along with a spin-coated device to make a clear comparison and analysis for self-assembled devices.

Two configurations of photodetectors were used, and a self-assembly process was then employed. The two configurations of photodetectors were horizontal/lateral, i.e., having electrodes separated by a horizontal distance, and the second one was vertical, which had electrodes separated vertically. The schematic of both configurations is shown in Figure 4.5.

We can also see the SEM image of the device in Figure 4.6. Using the recipe described above, a layer of NPLs, all in facedown orientation, was deposited on the device and the dummy silicon substrate. The SEM images are shown in Figure 4.7.

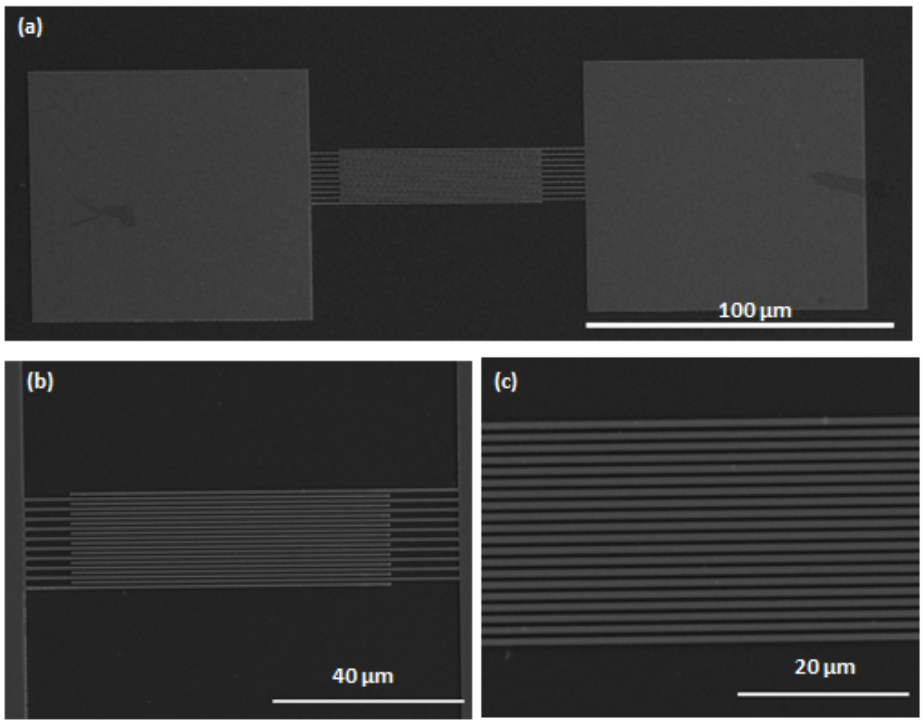

Figure 4.6: SEM images of the lateral device on Si-substrate: (a) the whole device, (b) and (c) the active region of interdigitated electrodes at different scales.

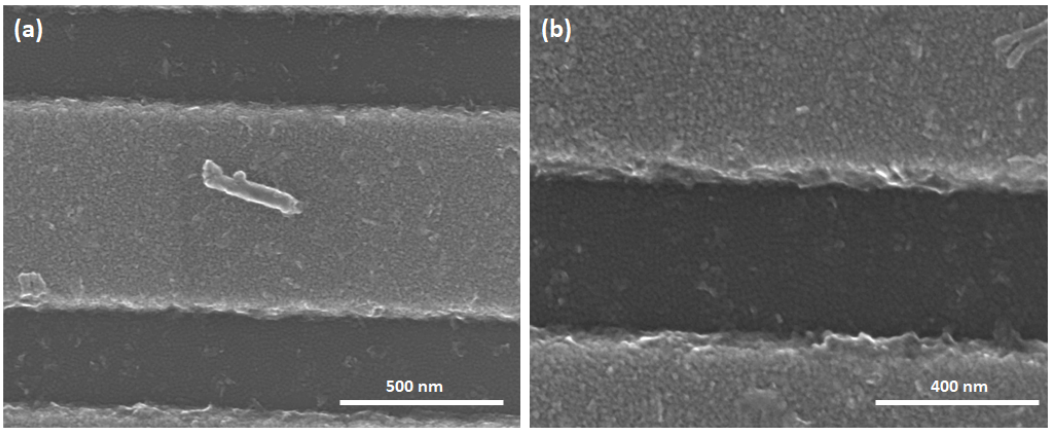

Figure 4.7: SEM images of the facedown self-assembly on the lateral device at (a) 500 nm and (b) 400 nm scale.

Repetitive steps for the facedown self-assembly can be used to build-up multilayered facedown structures and then can be employed in the device.

The other orientation, i.e., edgeup was also achieved using the same liquid interface technique by exploiting the evaporation rate of the solvent and the selection of subphase. To obtain the edgeup films, one has to wash the NPLs in the same way but this time disperse them in octane since octane evaporates more slowly than hexane. The optimized concentration that works well for the core NPLs is 20 mg/mL with the dropping volume as 20 μL. Notice that the concentration is decreased and the volume of dropping is increased. This aims at enhancing the alkane environment in the Teflon to induce slow evaporation of octane, which leads to edgeup orientation of NPLs. However, we must be careful, not to decrease the concentration too much, or else cracks will be formed and would damage the film quality. The Teflon used for edgeup self-assembly is smaller than for the facedown, i.e., 6 cm in diameter, since the evaporation rate will be further slowed when the surface area is reduced. Again, the same apparatus is used, but the subphase is ethylene glycol. From a macroscopic perspective, the two major interactions here are inter-NPLs and between NPLs and the subphase. If the subphase and the solvent have less polarity difference, then they tend to mix, and if the polarity difference is larger, then comparatively, they do not mix as such. The matching of polarities enhances the solubility of ligands, in the subphase and hence increases the interaction potential between NPLs and subphase, resulting in the facedown orientation of NPLs. In contrast, if the polarity difference is high, as in the case of octane and ethylene glycol, the ligands will not be soluble in the subphase and rather increases the chance of enhancing inter-NPL interaction which results in edgeup orientation. A similar explanation is given in [24].

Once the setup is ready, we pour ethylene glycol (EG) in the Teflon, drop 20 μL of the NPLs solution, and cover the Teflon instantly to perform the assembly in a closed environment. The Teflon is covered with a lid for almost 30 min here, to make sure that NPLs had enough time to orient themselves in edgeup orientation. This recipe is taken from [24] with some modifications. The SEM images for 4 ML CdSe core NPLs in edgeup assembly are shown in Figure 4.8.

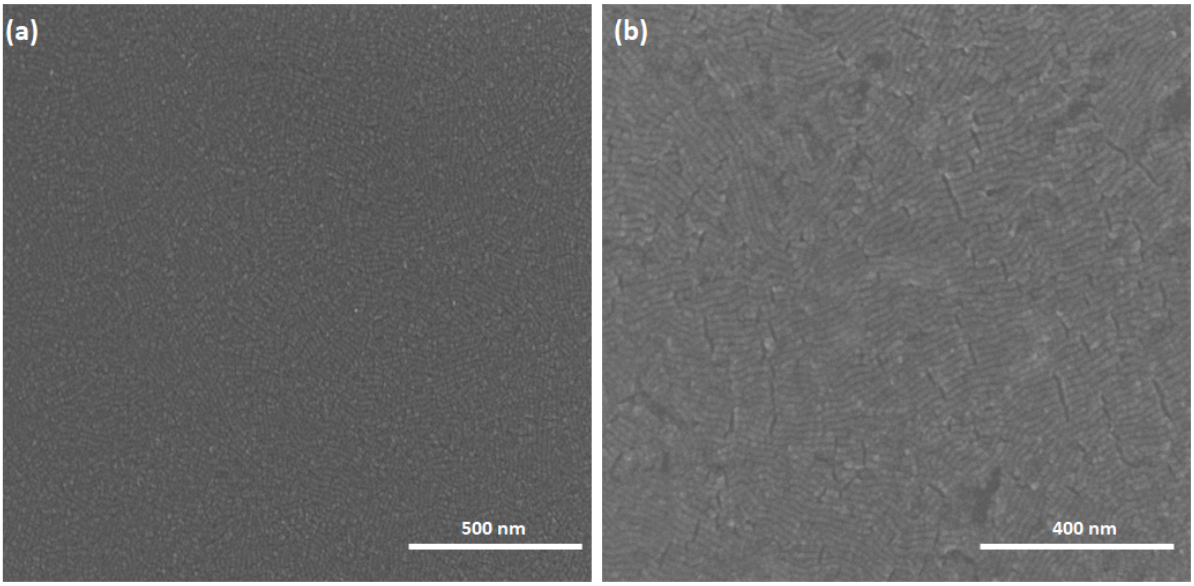

Figure 4.8: SEM images of the edgeup self-assembly with different (a) and (b) magnification scales.

The technique was repeated several times to check the reproducibility and the results were reproducible. Later on, the method was used to prepare the edgeup layer of the NPLs for the photodetectors of both configurations. The SEM results are shown in Figure 4.9.

Last, a spin-coated device was also fabricated as a negative control group to clearly see the impact of oriented self-assembly. The spin-coater was used in dynamic mode with 3,000 rpm. The SEM micrographs of the spin-coated layer on the Si-substrate and on the dummy device are shown in Figures 4.10 and 4.11, respectively.

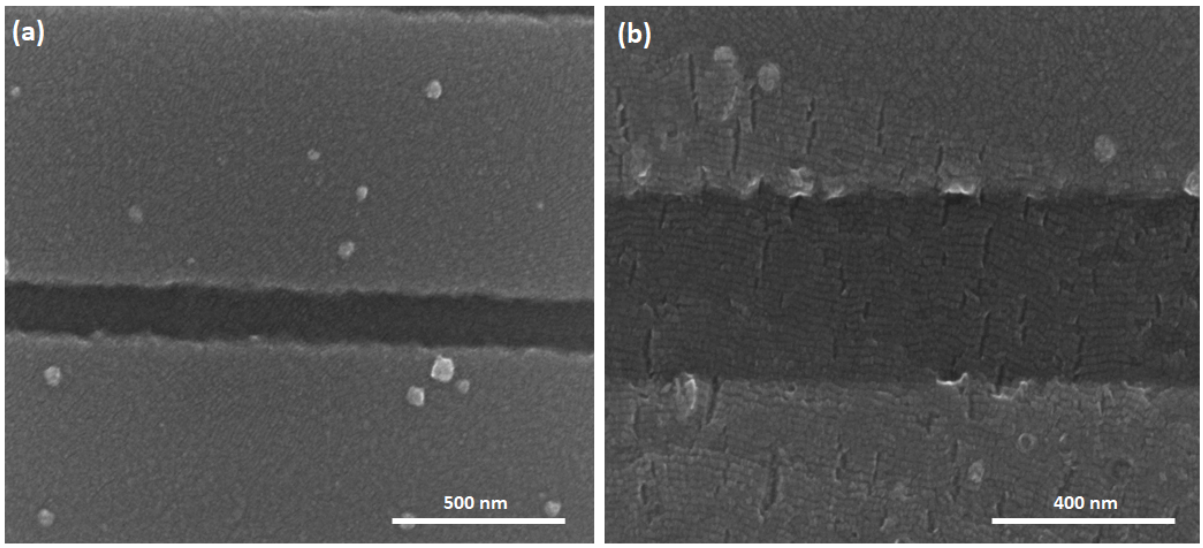

Figure 4.9: SEM images of the edgeup self-assembly on lateral dummy device with different (a) and (b) magnification scales.

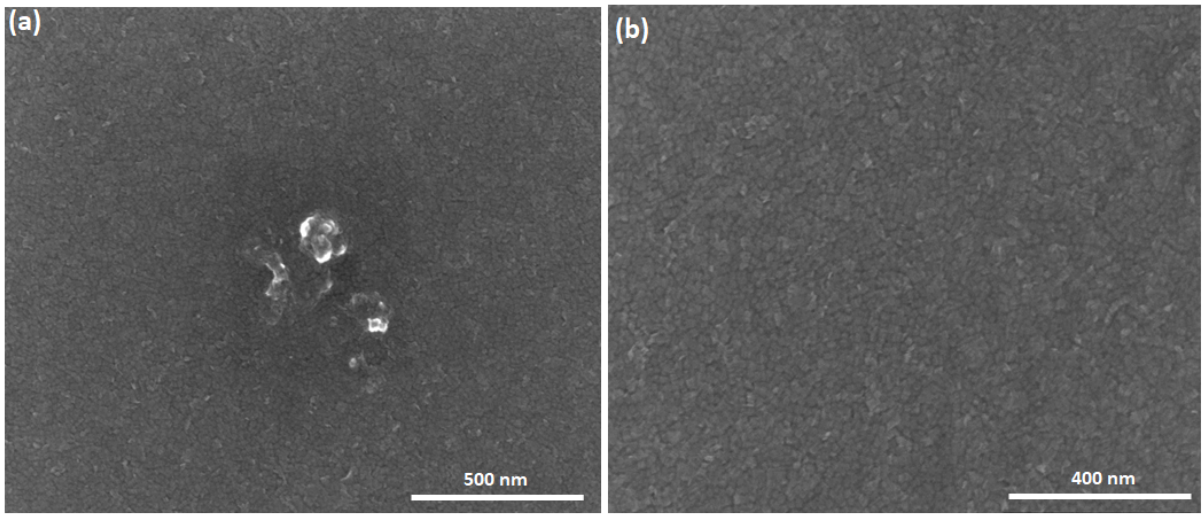

Figure 4.10: SEM images of the spin-coated NPLs on Si-substrate with different (a) and (b) scales.

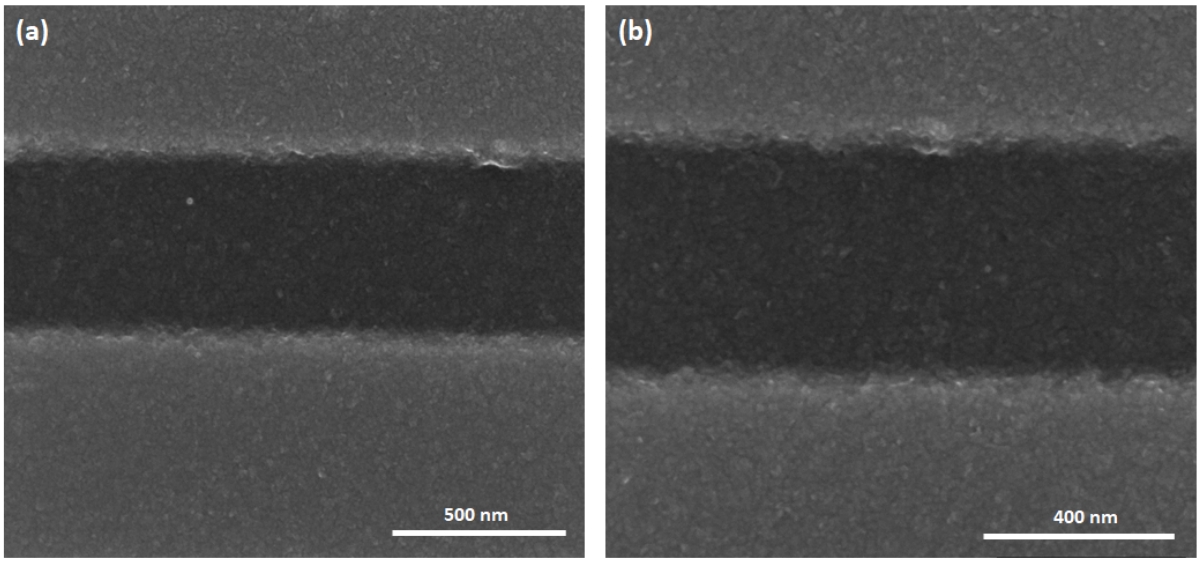

Figure 4.11: SEM images of the spin-coated NPLs on a lateral device with different (a) and (b) scales.

Here, it is worth noting that some images are unclear because the core NPLs are damaged under high-energy electrons striking them. Thus during imaging, in a very short span of time, their images need to be taken, and for the same reason, high magnification was not possible. However, the images will be clearer for core/shell NPLs, and assemblies can be analyzed in a better way.

4.1.2 4 ML CdSe/CdZnS Core/Shell NPLs

This material has been extensively utilized throughout this thesis at Demir's lab. The shells are usually deposited onto core structures to enhance the QY, to obtain a range of different colors of emitted light from the same material, to make them stable with surface passivation. Therefore, CdSe/CdZnS core/shell NPLs are used in devices such as LEDs, lasers and photodetectors. The optical characteristics of the material are shown in Figure 4.12.

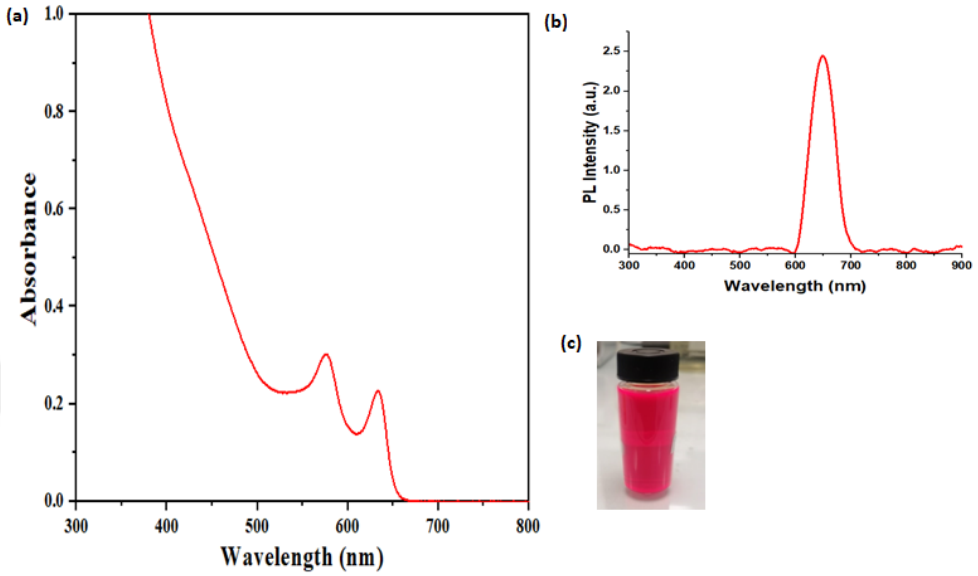

Figure 4.12: 4 ML CdSe core NPLs coated with CdZnS shell (a) absorption and (b) PL spectra around 645 nm, and (c) photograph of the sample.

In literature, the self-assembled films of 4 ML CdSe nanoplatelets are already found of much significance. Thanks to the quasi-2D structure of these nanoplatelets, their transition dipole moments (TDMs) lie parallel to the lateral dimensions of the nanoplatelets, and therefore, their self-assembled films with controlled orientations can play an important role in lighting devices such as LEDs [91]. We will talk in detail as we proceed in this chapter.

To achieve the self-assembly with core/shell along with NPLs, the material, and setup were prepared according to the recipe stated in the previous chapter. For the facedown self-assembly of the core/shell NPLs, the subphase used is ACN, the concentration of NPLs dispersed in hexane is 25 mg/mL, and the dropping volume is 10 μL in the teflon of 8 cm diameter. The Teflon is covered instantly to achieve a closed environment for the assembly. The SEM results are shown in Figure 4.13.

The recipe was repeated several times to check reproducibility and was then used for the preparation of the photodetector. The SEM images are given in Figure

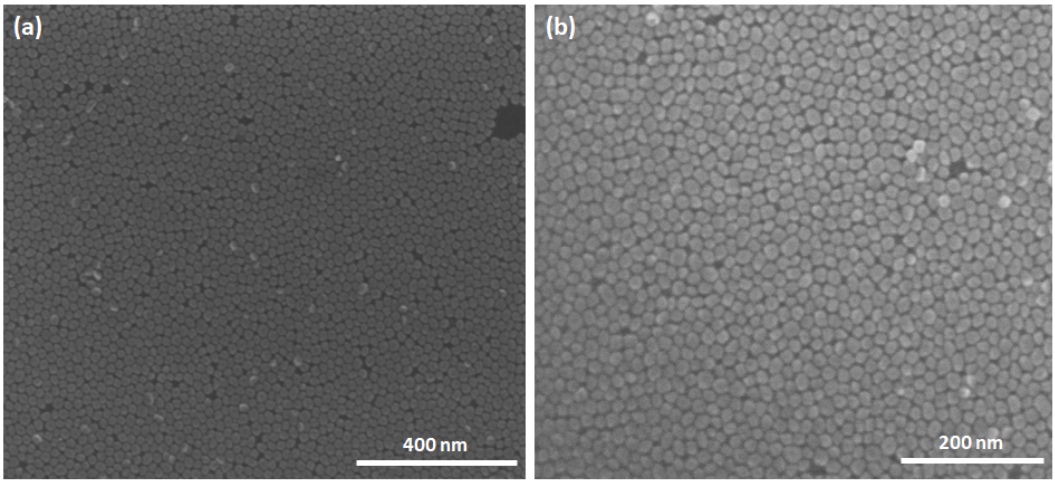

Figure 4.13: SEM micrographs of facedown self-assembled film of CdSe/CdZnS core/shell NPLs with different (a) and (b) scales.

4.14.

To obtain the edgeup film of core/shell NPLs, we repeated the same recipe as for the cores but at a slightly lower concentration, i.e., 17 mg/mL, but using the same dropping volume, i.e., 20 uL. The edgeup oriented film can be formed at the same concentration as for the cores, but this number works well mostly, again found by error and trial method. The lowering of concentration can be explained as the core/shell NPLs are heavier than the cores so a higher alkane environment would result in a better edgeup film. The edgeup films are then prepared in a closed environment with the same remaining steps as stated in the previous chapter. The SEM images of the films are shown in Figure 4.15. The recipe was then used to produce the edgeup film of core/shell NPLs in the photodetector device.

Using the same approach to make good and conclusive comparisons for the response time of the photodetectors, the spin-coated device was also prepared. The SEM images for spin-coated core/shell NPLs on a plane Si-substrate and on the dummy device are shown in Figures 4.16 and 4.17, respectively.

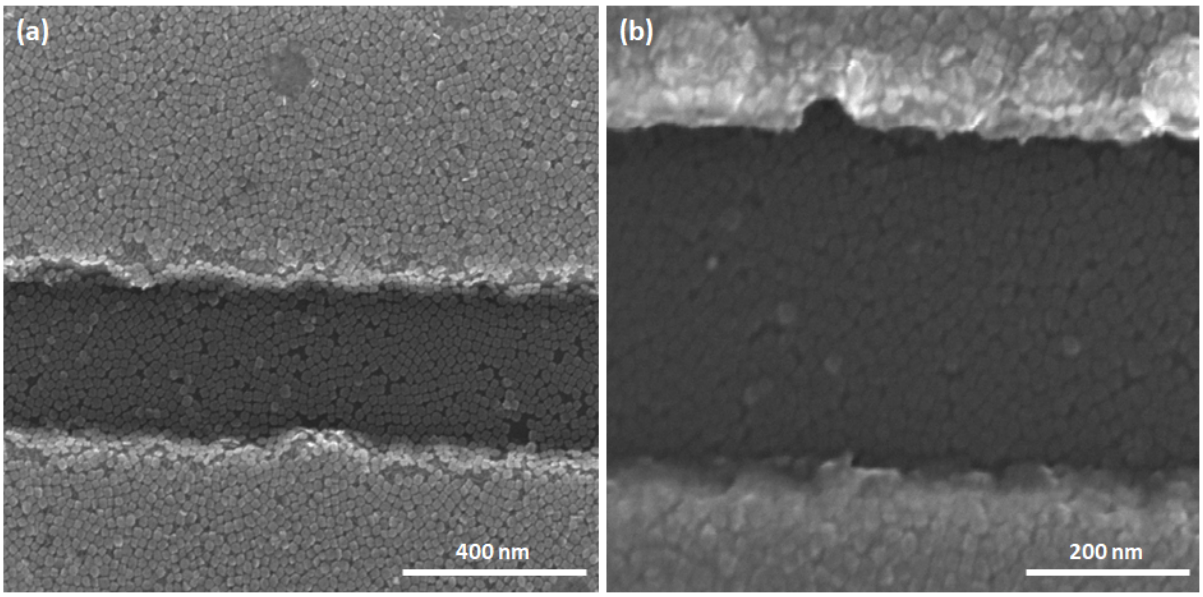

Figure 4.14: SEM micrographs of facedown self-assembled film of CdSe/CdZnS core/shell NPLs over and between the electrodes of the photodetector with different (a) and (b) magnification scales.

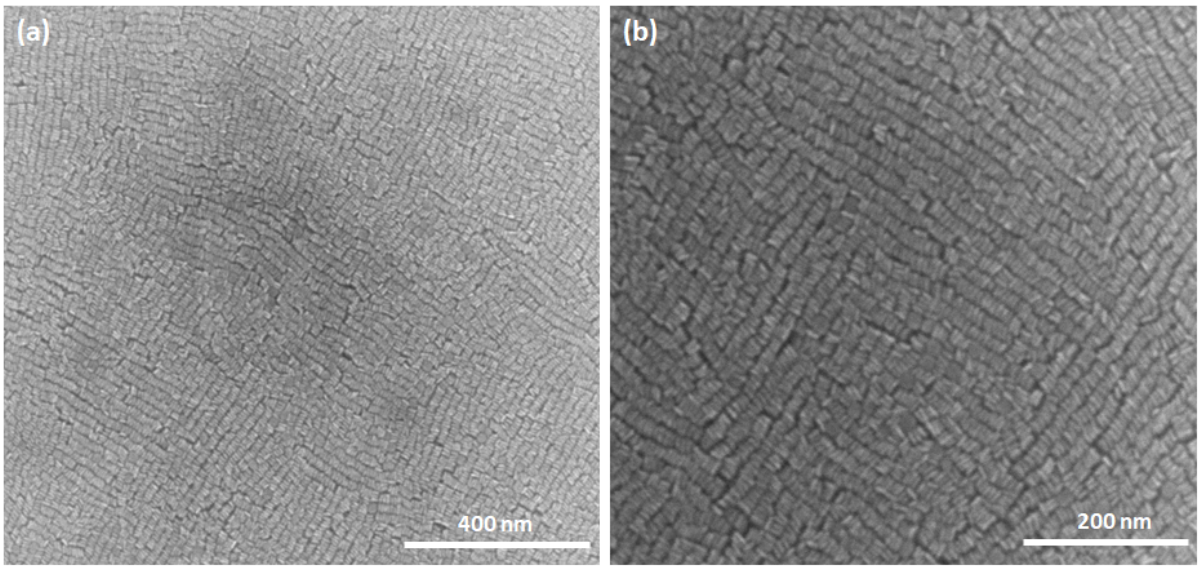

Figure 4.15: SEM micrographs of edgeup self-assembled film of CdSe/CdZnS core/shell NPLs on a Si-substrate with different (a) and (b) magnification scales.

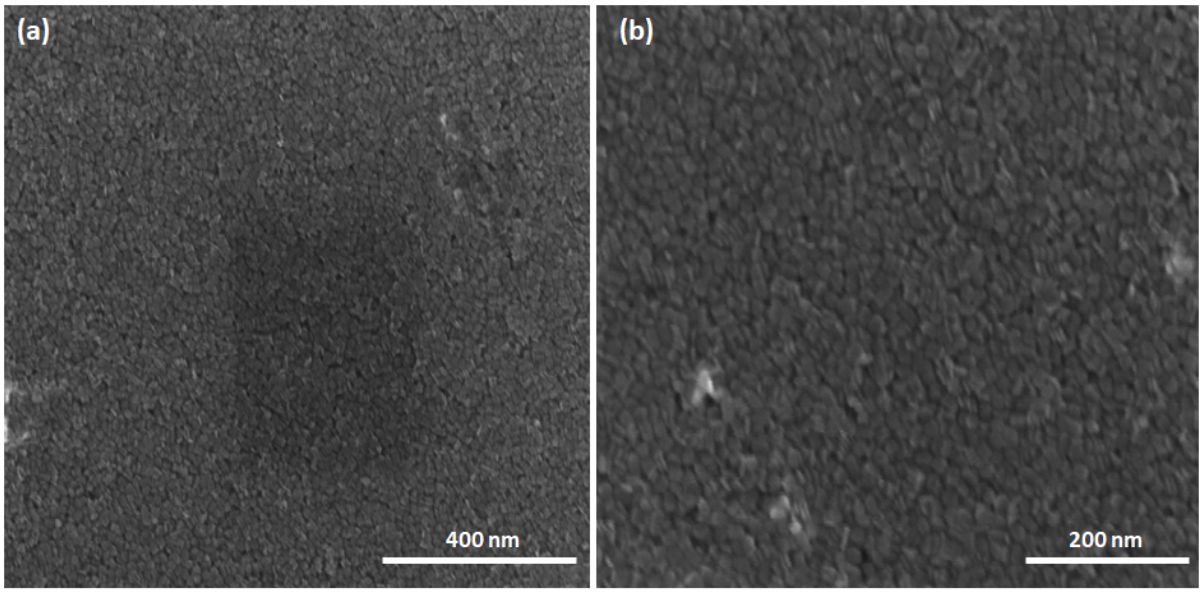

Figure 4.16: SEM micrographs of spin-coated CdSe/CdZnS core/shell NPLs on a Si-substrate with different (a) and (b) magnification scales.

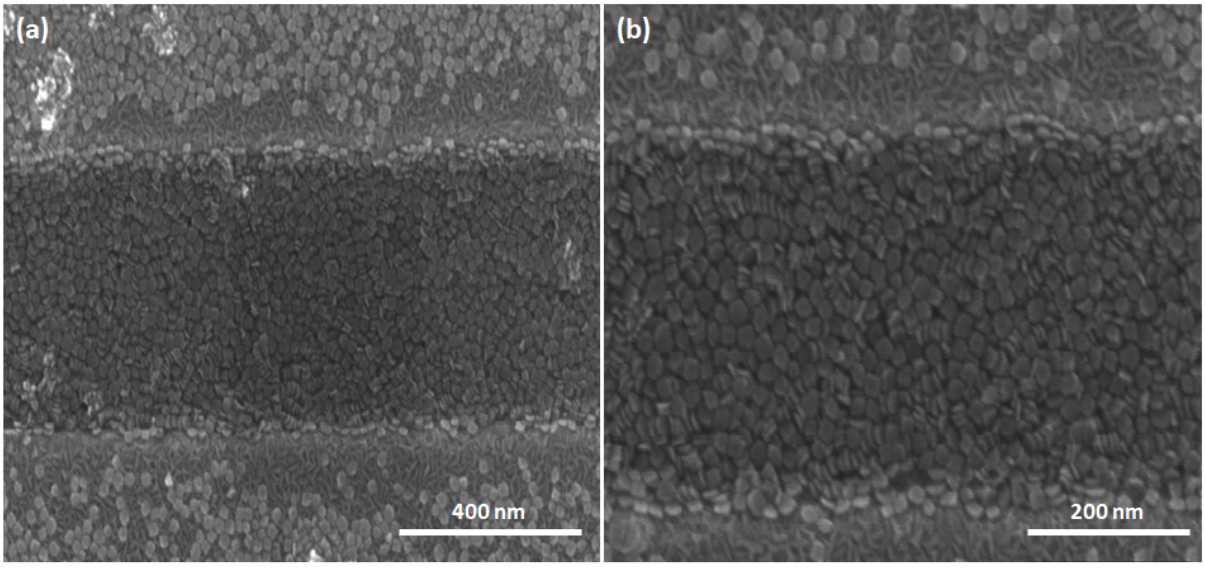

Figure 4.17: SEM micrographs of spin-coated CdSe/CdZnS core/shell NPLs over and between the electrodes of the photodetector with different (a) and (b) magnification scales.

Apart from the application of this self-assembly technique in photodetectors, we can also employ this for the deposition of active media of LED devices, as previously carried out by one of our group members, where the performance was enhanced due to the oriented self-assembly procedure. Since controlling the orientation of NPLs in the whole film allows enhanced directional emission compared to the mixed orientations. We will first analyze the BFP results of the three films: face-down, edge-up, and spin-coated to demonstrate the significance of the orientation-dictated self-assembly.

4.1.2.1 BFP Analysis of CdSe/CdZnS Core/Shell NPLs Films in Specific Orientation

The back-focal-plane images are useful for analyzing the emission patterns of the emitters as they provide the angular distributions of the emitted light. Furthermore, a BFP image can be viewed as the in-plane momentum of the emitted light (k_x and k_y), as the angular distribution is related to the light's momentum.
In the BFP setup is that a sample is excited with an incoming light source, producing a transition dipole moment due to excitation, and then emits due to the de-excitation process. The orientation and the radiation patterns of this dipole are important. The back-focal-plane is then imaged to extract the information from this emitted light which is passed through a defined polarization axis before entering the CCD camera.

The radiation pattern of NPLs is dumb-bell shaped, i.e., the shape of a p-orbital [92]. The BFP images of emissions from purely in-plane and out-of-plane dipoles are shown in Figures 4.18 and 4.19, respectively. In all the BFP images, the polarizer was parallel to the p-pol axis. Figures 4.18 and 4.19 are in agreement with [13].

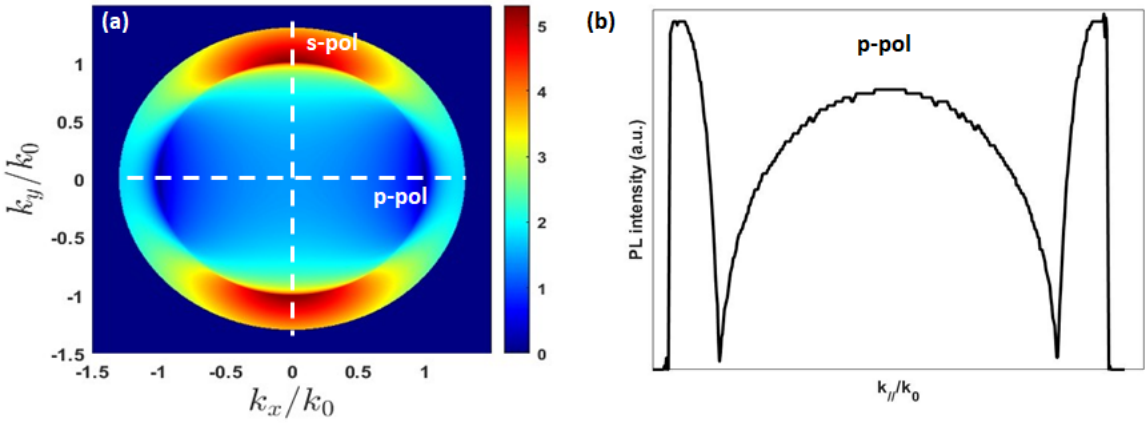

Figure 4.18: BFP image of (a) pure in-plane emitters and (b) intensity profile along p-polarization axis.

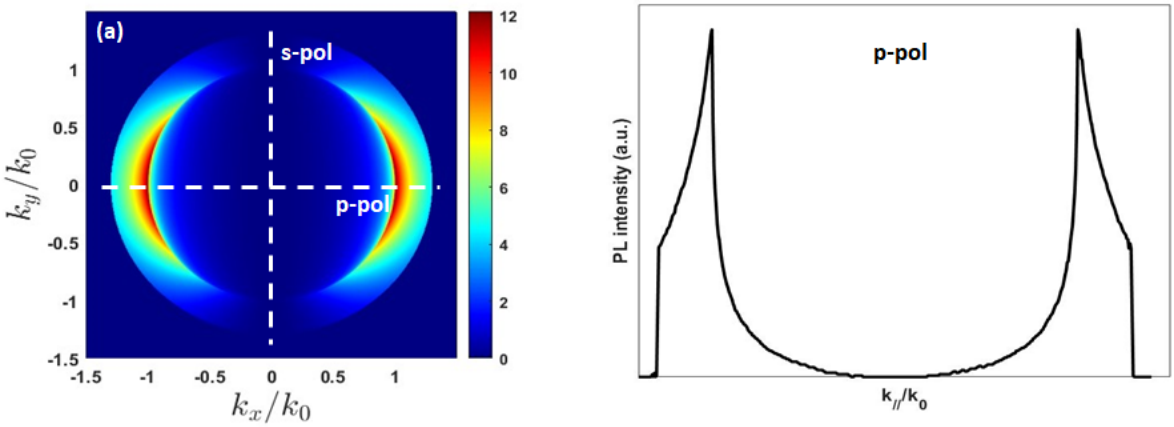

Figure 4.19: BFP image of (a) pure out-of-plane emitters and (b) intensity profile along p-polarization axis.

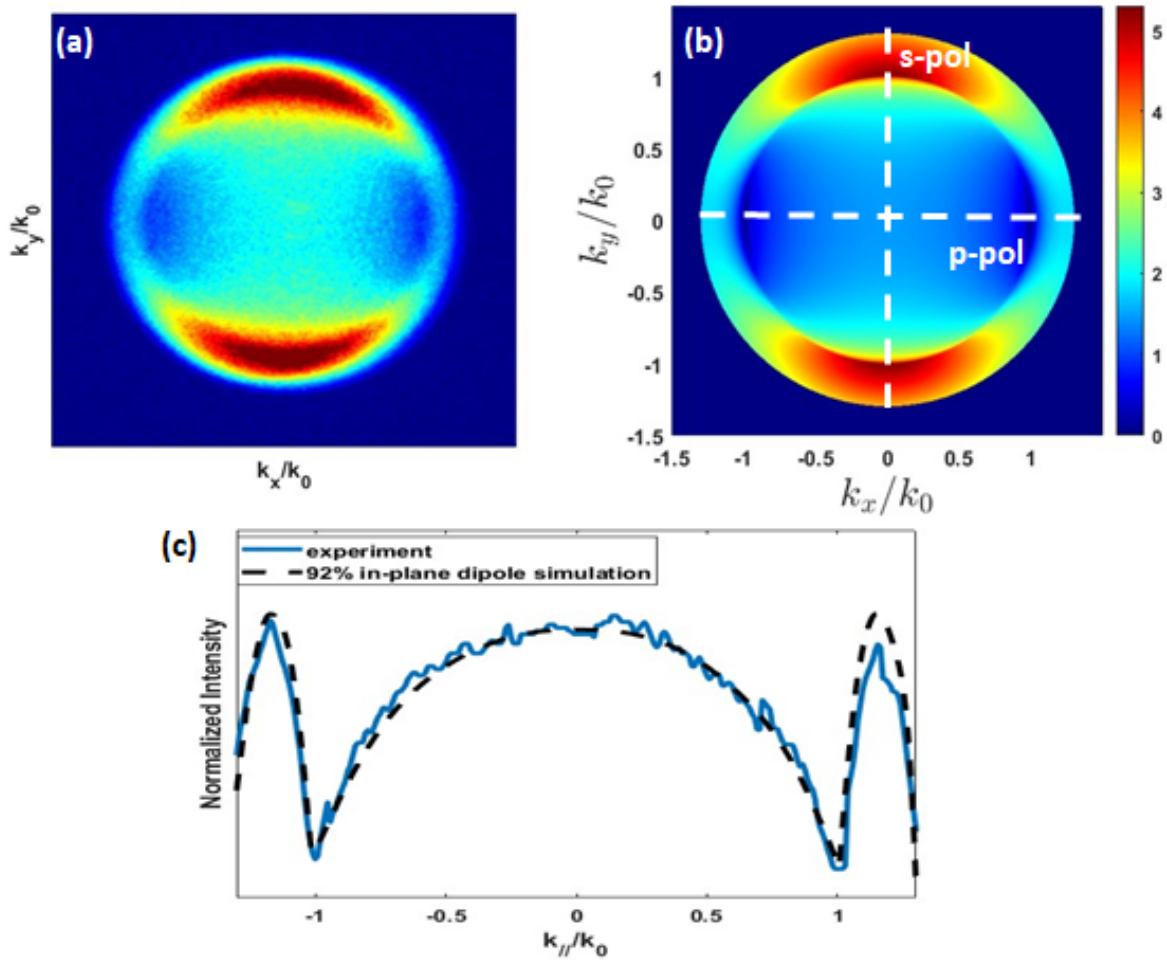

Figure 4.20: BFP results for the face-down self-assembled film: (a) experimental and (b) simulated map and (c) intensity plot along p-polarization axis.

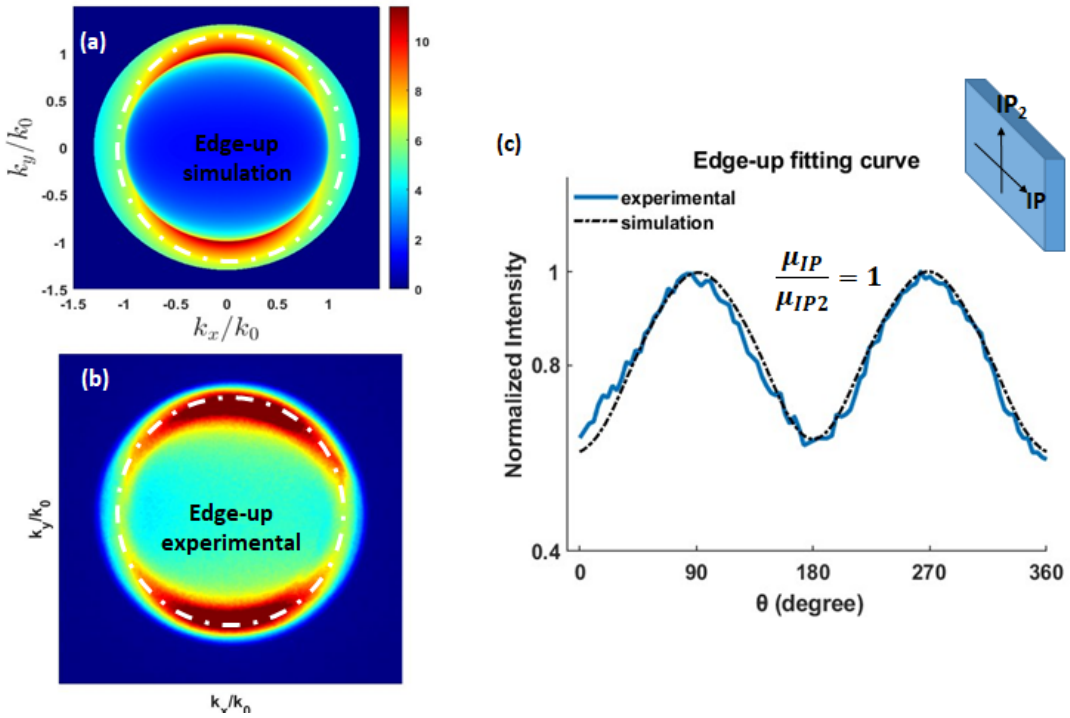

Figure 4.21: BFP results for the edge-up self-assembled film: (a) Simulation, (b) experimental data and (c) intensity distribution along the white dashed contour. The zero-theta value starts at $\frac{k_x}{k_0} = 1$.

The films were deposited on quartz substrates to analyze the BFP images of the oriented films. The BFP results for the face-down self-assembled film of 4 ML CdSe/CdZnS core/shell NPLs is shown in Figure 4.20. It is clear from the comparison of Figure 4.20 (a) and (b) that, in the face-down orientation, the transition dipoles are in-plane, yielding a directional emission that is highly required in lighting devices.

Similarly, the edge-up film was also deposited on quartz and then analyzed. The BFP results for the edge-up film are given in Figure. 4.21. To develop insight into the emission profile from edgeup film, first, we need to be clear about the terms in-plane and out-of-plane. Here these terms are used with reference to the plane of NPLs for the analysis. It can be clearly seen in Figures 4.21 (a) and (b) that the emission is not directional but rather there exists some emission which must

be due to the out-of-plane dipole emitters. The existence of these out-of-plane dipoles can be due to the stacking of NPLs and strain-induced NPL deformations. Still, these assemblies can be effective in devices such as photodetectors where charge transportation would be enhanced because of this orientation. The explanation is quite simple, as ligands are attached mostly to the facets, as compared to the edges, of these NPLs, and charge transportation occurs through these ligands, hence stacking orientation could help in faster charge transportation.

Last, a spin-coated film was also prepared for the BFP analysis. The results are shown in Figure 4.22. From Figure 4.22(c), it is found that 65% of the dipoles are in-plane, which was expected since the spin-coating technique results in a mixed orientation of NPLs. Thanks to our method for controlling the orientation of NPLs, the device applications from such oriented films can be further pushed forward.

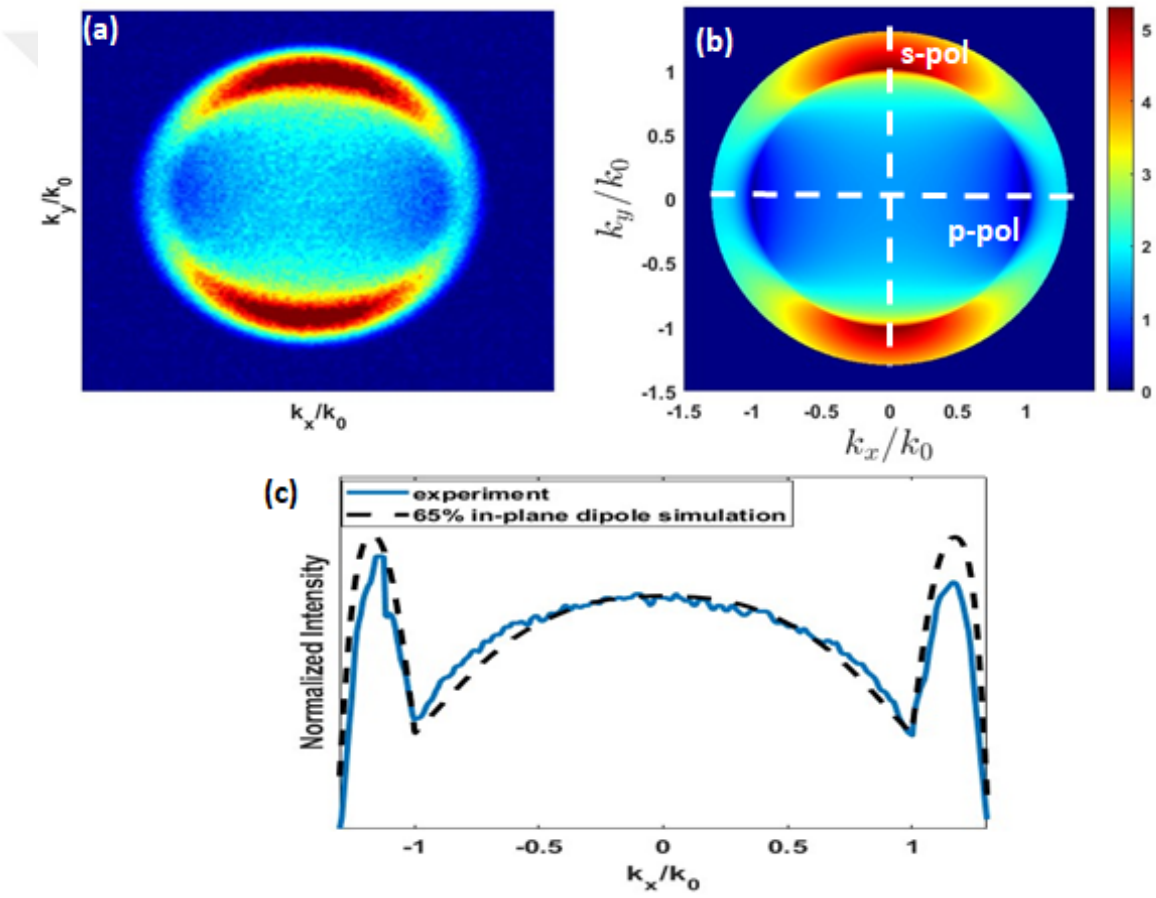

Figure 4.22: BFP results for the spin-coated film: (a) Experimental and (b) simulated maps (c) intensity along the p-polarization axis.

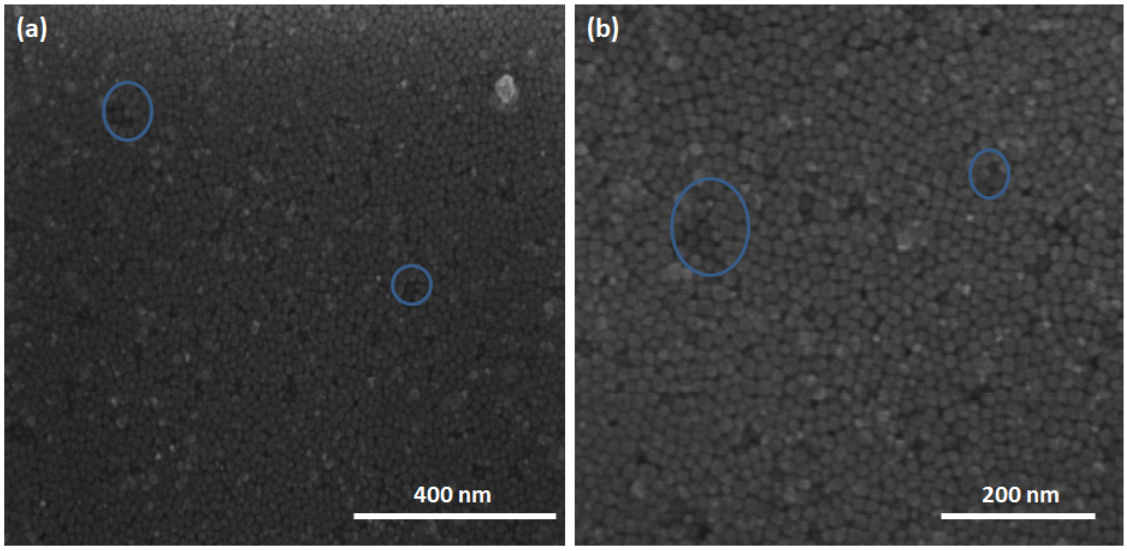

Figure 4.23: SEM micrographs of double-layered-facedown self-assembly of CdSe/CdZnS core/shell NPLs with different (a) and (b) scales.

The technique was also tested to prepare multi-layered and alternative layered superstructures of these oriented films either in fixed or altering orientation. The roughness of these films was analyzed using AFM. First, a double-layered-facedown structure was prepared using the same recipe sequentially. The rough patches were found, and SEM images were taken. The SEM image for the double-layered-facedown is shown in Figure 4.23. The encircled parts are the cracked parts, found on the top film where the orientation of the underneath film can be seen.

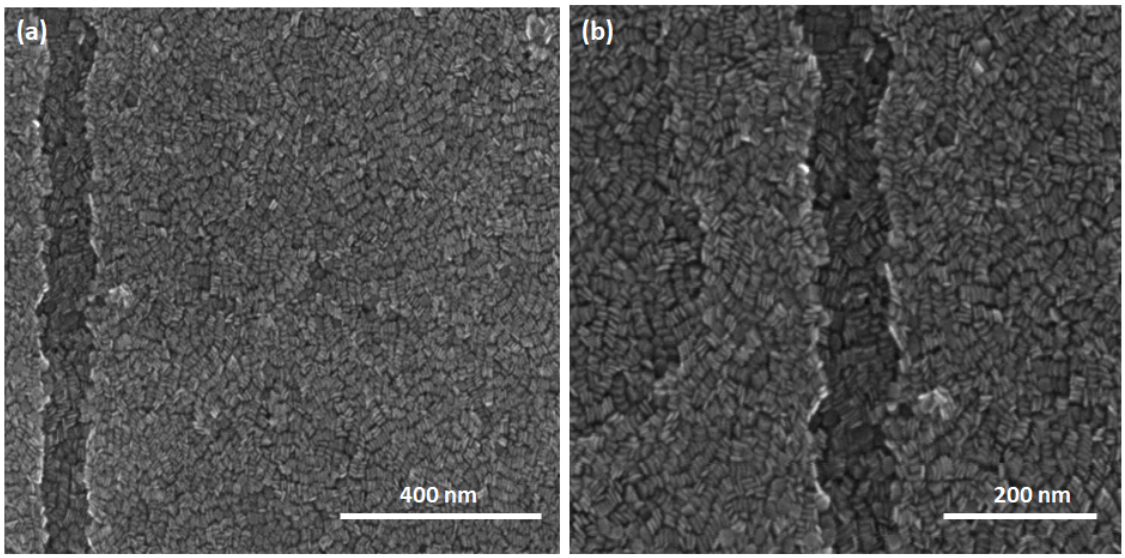

Figure 4.24: SEM images of double-layered-edgeup self-assembled CdSe/CdZnS core/shell NPLs with different (a) and (b) scales. Cracked regions are shown to conclude the orientation of the top and bottom layers.

By successively repeating the recipe of edge-up oriented film, a double-layered-edgeup film was formed. The SEM images where the film has cracks and rough patches are shown in Figure 4.24.

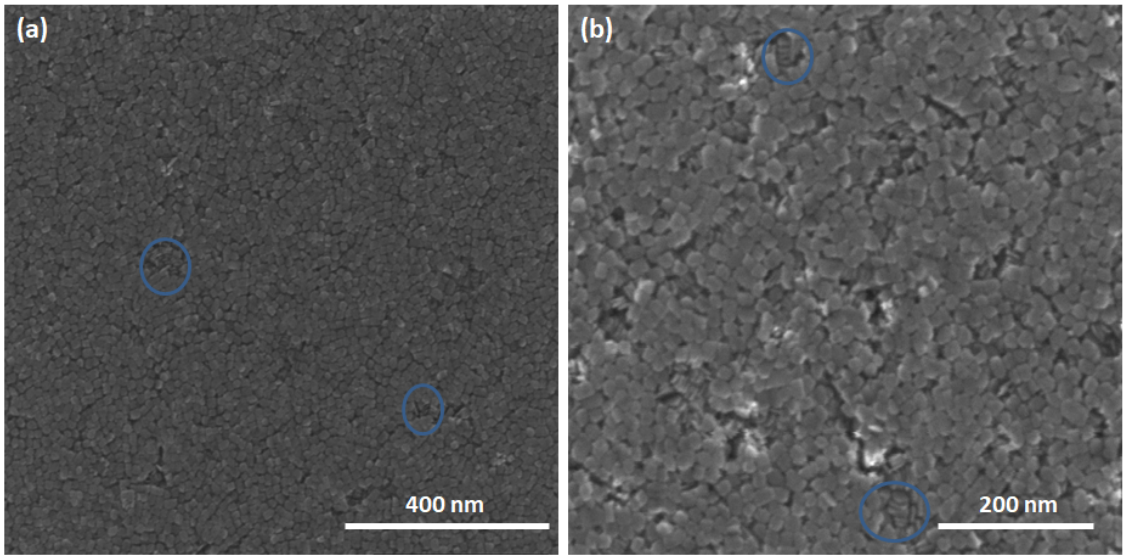

Figure 4.25: SEM micrographs of facedown-on-edgeup alternating orientation film of CdSe/CdZnS core/shell NPLs with different (a) and (b) scales. The encircled parts are marked to show the orientation of NPLs in the bottom layer.

Using the recipe for face-down and edge-up assembled films, alternatingly oriented superstructures were formed. These layers are facedown-on-edgeup and edgeup-on-facedown. The facedown-on-edgeup structure has a bottom layer in edgeup orientation and a top layer in the facedown orientation. The SEM images are shown in Figure 4.25.

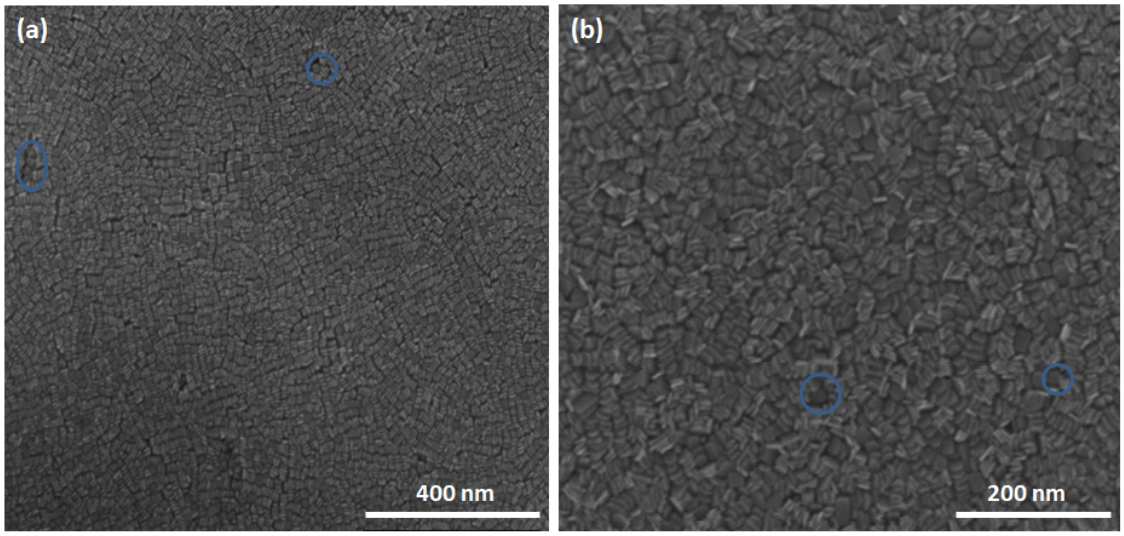

Figure 4.26: SEM micrographs of edgeup-on-facedown alternating orientation of CdSe/CdZnS core/shell NPLs with different (a) and (b) scales. The encircled parts are marked to show the orientation of NPLs in the bottom layer.

Similarly, the edgeup-on-facedown structure has a bottom layer of the face-down NPLs and a top layer of NPLs in the edge-up orientation. The SEM images of this structure are shown in Figure 4.26.

There is no doubt about the excellence of the technique, and surely, the structures formed can play an important role in device applications such as photodetectors, LEDs, and lasers. Before depositing the films as active layers of the devices, their surface roughness must be analyzed, especially in the devices where orientation is a key in enhancing performance. For this reason, the deposited films were analyzed with AFM for surface roughness. The 3D topology, along with S_q (RMS roughness), are given in Figures 4.27 and 4.28.

From the S_q values, we can see that the average roughness for all the films is around 2 nm which is excellent considering other nanoparticle deposition techniques.

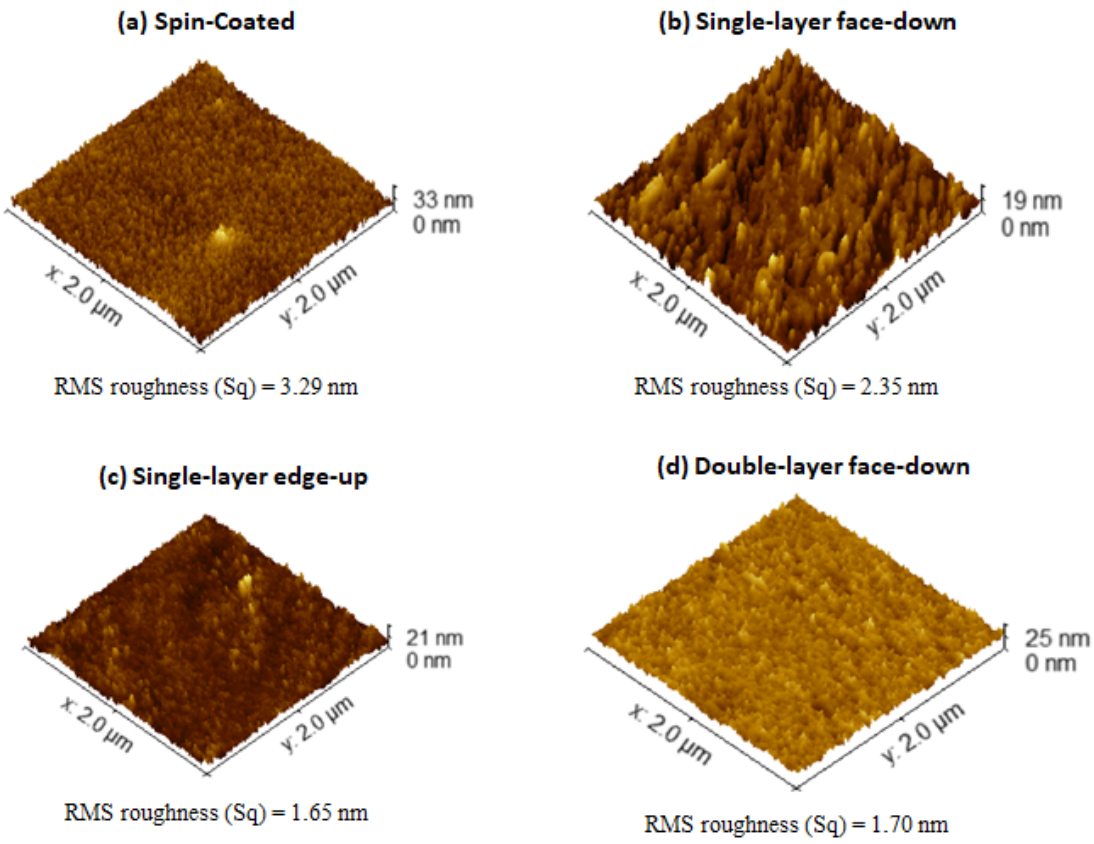

Figure 4.27: AFM micrographs showing 3D topologies along with S_q values of the prepared films: (a) spin-coated, (b) single-layer face-down, (c) single-layer edge-up, and (d) double-layer face-down films.

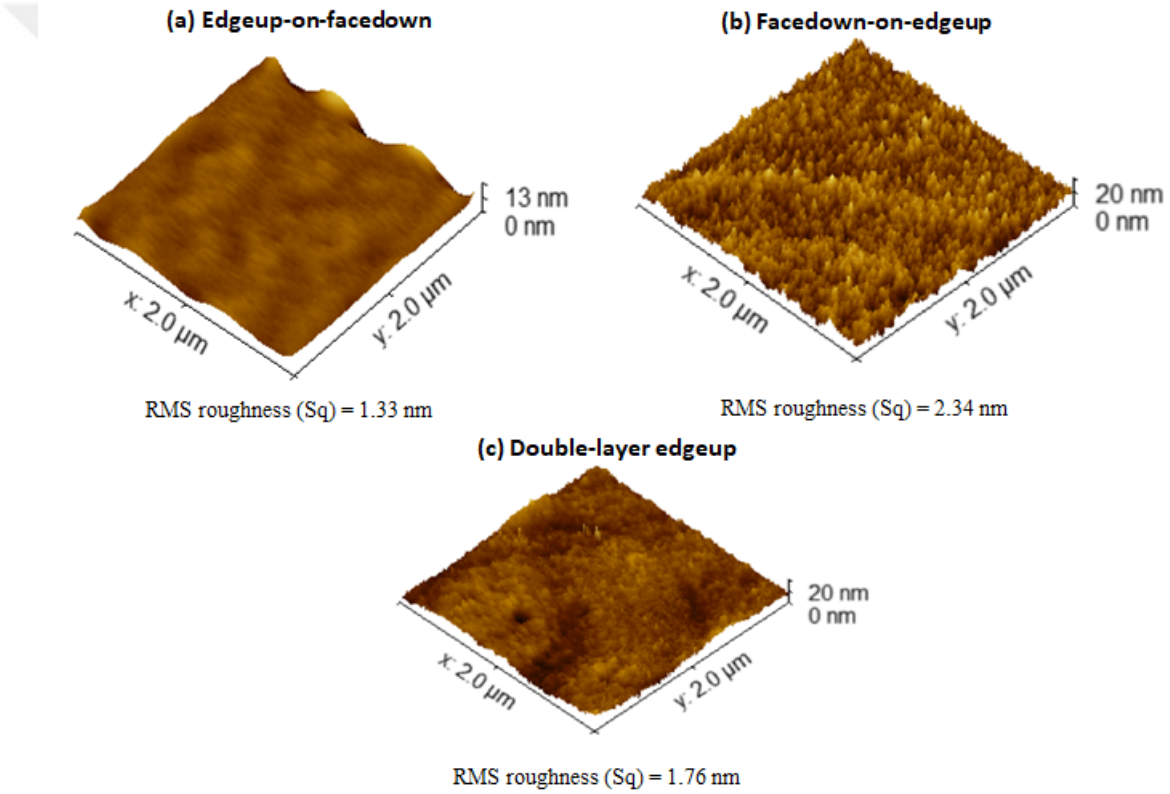

Figure 4.28: AFM micrographs showing 3D topologies along with S_q values of the prepared films: (a) edgeup-on-facedown, (b) facedown-on-edgeup, and (d) double-layer edge-up films.

This technique is not restricted to the deposition of usual-sized NPLs; rather, it can also be applied to deposit large NPLs and cubic QDs. In the next section, we will present these results.

4.1.3 Copper-Indium-Sulfide (CIS) NPLs

These are hexagonal nanoplatelets that are large in their lateral size(80 to 100 nm). In this section, we will see the results of the self-assembled layer of these large NPLs using the same liquid-interface self-technique.

To perform the self-assembly, the setup was constructed as for all previous assemblies. The material was washed using acetone and redispersed in toluene with an optimized concentration of 28 mg/mL. These NPLs are not much stable in hexane dispersion but comparatively more stable in toluene, probably because of their size. Last, ethylene glycol was poured into the teflon well of 8 cm in size, and a volume of 10 μL of the optimized solution was dropped on the side of the well. The teflon was covered instantly, and after 5 min, the subphase was pulled, and the sample was kept in the desiccator for controlled drying. The SEM micrographs of the assembly are shown in Figure 4.29.

Once the oriented self-assembled layer is achieved, as in Figure 4.29, it can be further utilized to study the material and its film characteristics for further applications in devices such as photodetectors. Along with photodetectors, this technique can be deployed further to study the energy transfer mechanisms of the material.

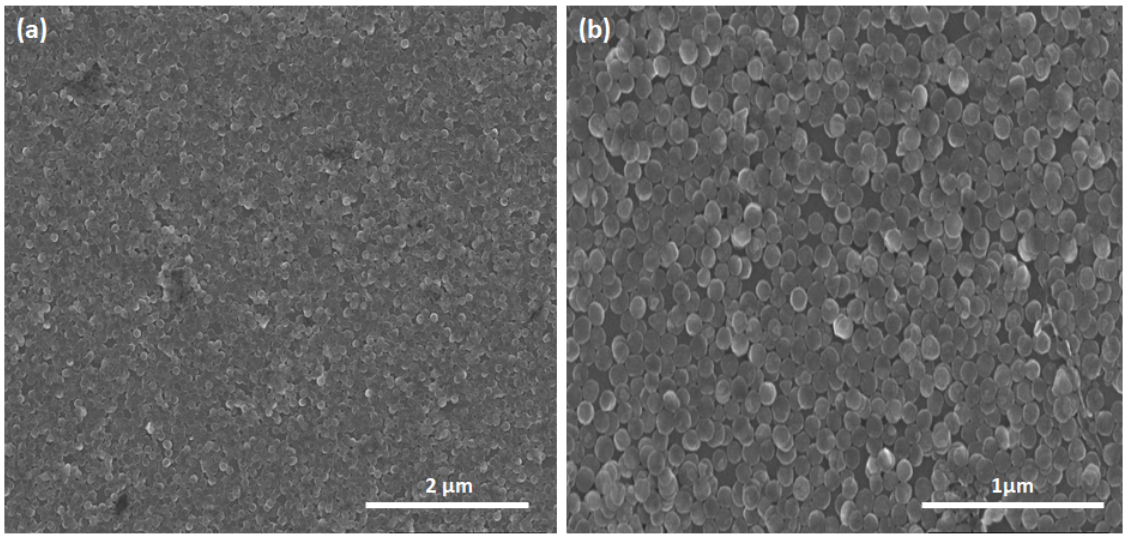

Figure 4.29: SEM micrographs of the face-down self-assembly of large hexagonal CIS NPLs with different (a) and (b) scales.

4.2 Cubic Core/Shell CdSe/CdZnS QDs

Here in this work, we have deposited single and multiple layers of cubic core/shell CdSe/CdZnS quantum dots. Since these are isotropic materials, so there is no specific orientation along which the particles were self-assembled.

To do so, we prepared the setup in the same way as for previous assemblies. We washed the material with methanol and redispersed it in hexane with an optimized concentration of 30 mg/mL in a teflon well of 6 cm in diameter. Finally, ACN was poured into the teflon, and 15 μL of the volume was dropped on the sidewall of the teflon. The teflon was covered instantly, and after a wait of 5 min, the subphase was pulled with a syringe. Finally, the sample was kept in the desiccator for controlled drying.

The SEM images of single-and multi-layered self-assembled films of cubic QDs are shown in Figures 4.30 and 4.31, respectively.

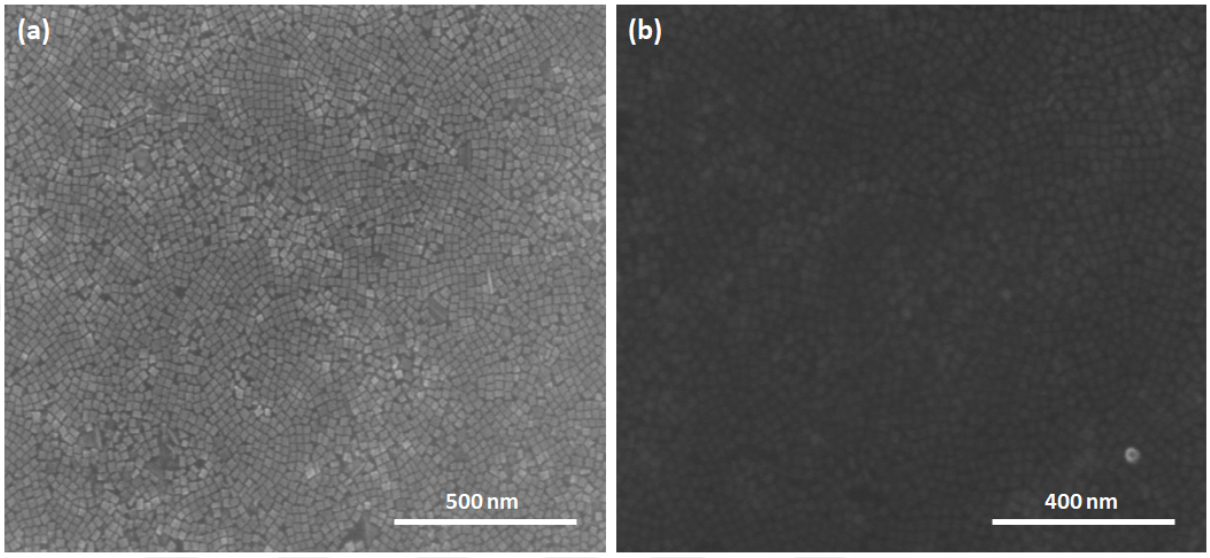

Figure 4.30: SEM micrographs of the self-assembled single-layer of cubic core/shell QDs with different (a) and (b) scales.

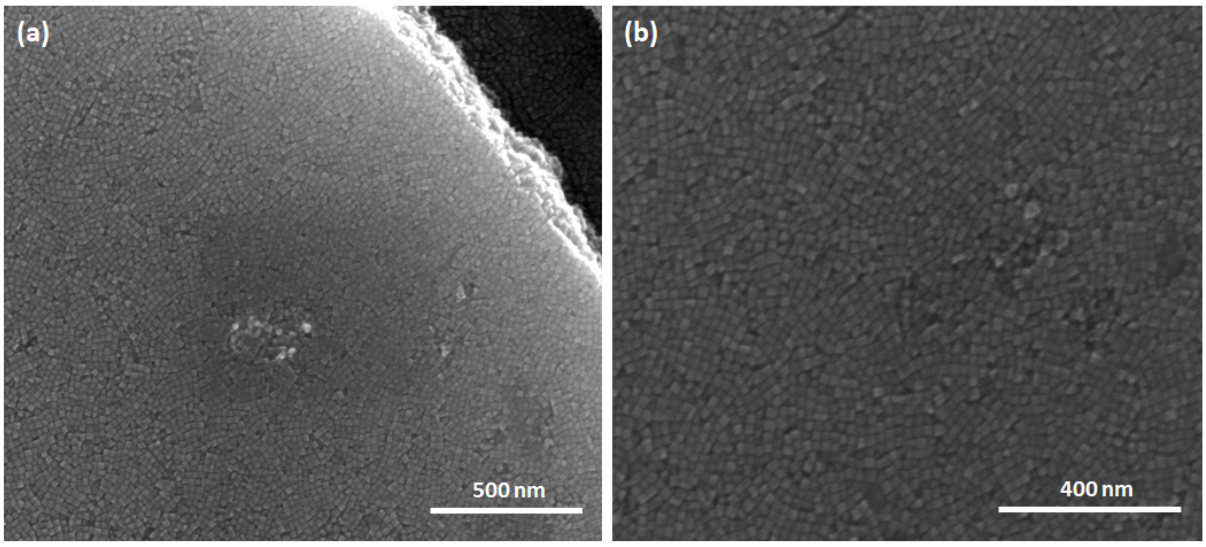

Figure 4.31: SEM micrographs of the self-assembled multi-layers of cubic core/shell QDs with different (a) and (b) scales.

Thus, we have seen the effectiveness of this technique, with our simple setup, in dictating the orientation of the anisotropic nanocrystals along with their self-assembly, as well as the self-assembly of isotropic nanocrystals and large hexagonal-shaped NCs.

Chapter 5

Conclusion

In this work, we have used the liquid-liquid interface self-assembly technique for the NCs dispersed in an apolar solvent and dropped over a polar subphase to self-assemble in a controlled environment. This technique has allowed us to dictate the orientation of anisotropic NCs, such as NPLs, exploiting the evaporation rate of the solvent in which NCs are dispersed.

The material used for the self-assembly was 4 ML CdSe cores and CdSe/CdZnS core/shell NPLs, synthesized and optically characterized using PL spectroscopy. The NPLs were self-assembled using our technique with their orientation control. The method was not limited to the deposition of a single oriented layer; but multi-layered structures with different orientations can be deposited up to an area of several cm^2. The surface morphology for all the films was then analyzed using the scanning electron microscopy. The BFP imaging was carried out over the oriented self-assembled layers to show the intrinsic novelty of these NPL films with specific orientations. Lastly, the surface roughness of the deposited films was analyzed using AFM, indicating that, the deposited film roughness on average, using this self-assembly technique was around 2 nm, which is considered a smooth surface.

Moreover, the technique has also been deployed to deposit the active layers of

photodetectors, in both lateral and vertical configurations, with both core and core/shell NPLs, where the response time is expected to be enhanced for the oriented films, rather than randomly oriented films of NCs.

Interestingly, the liquid-liquid interface self-assembly technique is not limited to self-assemble usual NPLs, but also to self-assemble large hexagonal-shaped NPLs and cubic QDs. As the device applications have not been included in the work of this thesis, and instead, the focus has been on the preparation of single-layered and multilayered oriented films, their device applications, along with back focal plane analysis, will follow as the future research steps. These devices will include both LEDs and photodetectors.

Bibliography

[1] C. Murray, D. J. Norris, and M. G. Bawendi, "Synthesis and characterization of nearly monodisperse cde (e= sulfur, selenium, tellurium) semiconductor nanocrystallites," *Journal of the American Chemical Society*, vol. 115, no. 19, pp. 8706–8715, 1993.

[2] A. L. Rogach, D. V. Talapin, E. V. Shevchenko, A. Kornowski, M. Haase, and H. Weller, "Organization of matter on different size scales: Monodisperse nanocrystals and their superstructures," *Advanced Functional Materials*, vol. 12, no. 10, pp. 653–664, 2002.

[3] V. Klimov, A. Mikhailovsky, S. Xu, *et al.*, "Optical gain and stimulated emission in nanocrystal quantum dots," *Science*, vol. 290, no. 5490, pp. 314–317, 2000.

[4] B. Guzelturk, Y. Kelestemur, M. Olutas, S. Delikanli, and H. V. Demir, "Amplified spontaneous emission and lasing in colloidal nanoplatelets," *ACS Nano*, vol. 8, no. 7, pp. 6599–6605, 2014.

[5] V. L. Colvin, M. C. Schlamp, and A. P. Alivisatos, "Light-emitting diodes made from cadmium selenide nanocrystals and a semiconducting polymer," *Nature*, vol. 370, no. 6488, pp. 354–357, 1994.

[6] B. Liu, Y. Altintas, L. Wang, *et al.*, "Record high external quantum efficiency of 19.2% achieved in light-emitting diodes of colloidal quantum wells enabled by hot-injection shell growth," *Advanced Materials*, vol. 32, no. 8, p. 1 905 824, 2020.

[7] T.-H. Kim, K.-S. Cho, E. K. Lee, *et al.*, "Full-colour quantum dot displays fabricated by transfer printing," *Nature Photonics*, vol. 5, no. 3, pp. 176–182, 2011.

[8] S. Ithurria and B. Dubertret, "Quasi 2d colloidal cdse platelets with thicknesses controlled at the atomic level," *Journal of the American Chemical Society*, vol. 130, no. 49, pp. 16 504–16 505, 2008.

[9] S. Ithurria, M. Tessier, B. Mahler, R. Lobo, B. Dubertret, and A. L. Efros, "Colloidal nanoplatelets with two-dimensional electronic structure," *Nature Materials*, vol. 10, no. 12, pp. 936–941, 2011.

[10] M. D. Tessier, C. Javaux, I. Maksimovic, V. Loriette, and B. Dubertret, "Spectroscopy of single cdse nanoplatelets," *ACS Nano*, vol. 6, no. 8, pp. 6751–6758, 2012.

[11] M. D. Tessier, P. Spinicelli, D. Dupont, G. Patriarche, S. Ithurria, and B. Dubertret, "Efficient exciton concentrators built from colloidal core/crown cdse/cds semiconductor nanoplatelets," *Nano Letters*, vol. 14, no. 1, pp. 207–213, 2014.

[12] J. Liu, L. Guillemeney, A. Choux, A. Maıtre, B. Abécassis, and L. Coolen, "Fourier-imaging of single self-assembled cdse nanoplatelet chains and clusters reveals out-of-plane dipole contribution," *ACS Photonics*, vol. 7, no. 10, pp. 2825–2833, 2020.

[13] Y. Gao, M. C. Weidman, and W. A. Tisdale, "Cdse nanoplatelet films with controlled orientation of their transition dipole moment," *Nano Letters*, vol. 17, no. 6, pp. 3837–3843, 2017.

[14] W. D. Kim, D. Kim, D.-E. Yoon, *et al.*, "Pushing the efficiency envelope for semiconductor nanocrystal-based electroluminescence devices using anisotropic nanocrystals," *Chemistry of Materials*, vol. 31, no. 9, pp. 3066–3082, 2019.

[15] A. Antanovich, A. Prudnikau, A. Matsukovich, A. Achtstein, and M. Artemyev, "Self-assembly of cdse nanoplatelets into stacks of controlled size induced by ligand exchange," *The Journal of Physical Chemistry C*, vol. 120, no. 10, pp. 5764–5775, 2016.

[16] M. Achermann, M. A. Petruska, S. A. Crooker, and V. I. Klimov, "Picosecond energy transfer in quantum dot langmuir- blodgett nanoassemblies," *The Journal of Physical Chemistry B*, vol. 107, no. 50, pp. 13 782–13 787, 2003.

[17] T. Ozel, S. Nizamoglu, M. A. Sefunc, *et al.*, "Anisotropic emission from multilayered plasmon resonator nanocomposites of isotropic semiconductor quantum dots," *ACS Nano*, vol. 5, no. 2, pp. 1328–1334, 2011.

[18] F. Kim, S. Kwan, J. Akana, and P. Yang, "Langmuir- blodgett nanorod assembly," *Journal of the American Chemical Society*, vol. 123, no. 18, pp. 4360–4361, 2001.

[19] I. Patla, S. Acharya, L. Zeiri, J. Israelachvili, S. Efrima, and Y. Golan, "Synthesis, two-dimensional assembly, and surface pressure-induced coalescence of ultranarrow pbs nanowires," *Nano Letters*, vol. 7, no. 6, pp. 1459–1462, 2007.

[20] I. Suarez, R. Munoz, V. Chirvony, *et al.*, "Multilayers of cdse/cds/zncds core/wings/shell nanoplatelets integrated in a polymer waveguide," *IEEE Journal of Selected Topics in Quantum Electronics*, vol. 23, no. 5, pp. 1–8, 2017.

[21] B. Martin-Garcia and M. M. Velázquez, "Nanoparticle self-assembly assisted by polymers: The role of shear stress in the nanoparticle arrangement of langmuir and langmuir–blodgett films," *Langmuir*, vol. 30, no. 2, pp. 509–516, 2014.

[22] T. Alejo, M. Merchán, M. Velázquez, and J. Pérez-Hernández, "Polymer/surfactant assisted self-assembly of nanoparticles into langmuir–blodgett films," *Materials Chemistry and Physics*, vol. 138, no. 1, pp. 286–294, 2013.

[23] C. Damle, A. Gole, and M. Sastry, "Multilayer langmuir–blodgett assemblies of hydrophobized cds nanoparticles by organization at the air–water interface," *Journal of Materials Chemistry*, vol. 10, no. 6, pp. 1389–1393, 2000.

[24] R. Momper, H. Zhang, S. Chen, *et al.*, "Kinetic control over self-assembly of semiconductor nanoplatelets," *Nano Letters*, vol. 20, no. 6, pp. 4102–4110, 2020.

[25] S. Volk, N. Yazdani, and V. Wood, "Manipulating electronic structure from the bottom-up: Colloidal nanocrystal-based semiconductors," *The Journal of Physical Chemistry Letters*, vol. 11, no. 21, pp. 9255–9264, 2020.

[26] P. J. Lu and D. A. Weitz, "Colloidal particles: Crystals, glasses, and gels," *Annu. Rev. Condens. Matter Phys.*, vol. 4, no. 1, pp. 217–233, 2013.

[27] E. Kraemer and S. T. Dexter, "The light-scattering capacity (tyndall effect) and colloidal behavior of gelatine sols and gels," *The Journal of Physical Chemistry*, vol. 31, no. 5, pp. 764–782, 2002.

[28] J. de Swaan Arons and G. Diepen, "Immiscibility of gases. the system hexe," *Recueil des Travaux Chimiques des Pays-Bas*, vol. 82, no. 8, pp. 806–806, 1963.

[29] M. Cahay, "Quantum confinement vi: Nanostructured materials and devices: Proceedings of the international symposium," The Electrochemical Society, 2001.

[30] A. P. Alivisatos, "Semiconductor clusters, nanocrystals, and quantum dots," *Science*, vol. 271, no. 5251, pp. 933–937, 1996.

[31] D. J. Griffiths and D. F. Schroeter, *Introduction to quantum mechanics*. Cambridge University Press, 2018.

[32] C. Kittel, *Introduction to solid state physics*. John Wiley & Sons, inc, 2005.

[33] M. C. T. Saleh Bahaa E, *Fundamentals of photonics*, 2007.

[34] S. V. Gaponenko, *Introduction to nanophotonics*. Cambridge University Press, 2010.

[35] O. Erdem, "Colloidal optoelectronics of self-assembled quantum well superstructures," Ph.D. dissertation, Bilkent Universitesi (Turkey), 2020.

[36] J. A. McGuire, J. Joo, J. M. Pietryga, R. D. Schaller, and V. I. Klimov, "New aspects of carrier multiplication in semiconductor nanocrystals," *Accounts of Chemical Research*, vol. 41, no. 12, pp. 1810–1819, 2008.

[37] P. Kambhampati, "Hot exciton relaxation dynamics in semiconductor quantum dots: Radiationless transitions on the nanoscale," *The Journal of Physical Chemistry C*, vol. 115, no. 45, pp. 22 089–22 109, 2011.

[38] S. Dey and Y. S. Jain, "On the wave mechanics of a particle in two different impenetrable spherical cavities," *arXiv preprint arXiv:1002.4308*, 2010.

[39] R. Dingle, W. Wiegmann, and C. H. Henry, "Quantum states of confined carriers in very thin al x ga 1- x as-gaas-al x ga 1- x as heterostructures," *Physical Review Letters*, vol. 33, no. 14, p. 827, 1974.

[40] L. E. Brus, "Electron–electron and electron-hole interactions in small semiconductor crystallites: The size dependence of the lowest excited electronic state," *The Journal of Chemical Physics*, vol. 80, no. 9, pp. 4403–4409, 1984.

[41] A. I. Ekimov, A. L. Efros, and A. A. Onushchenko, "Quantum size effect in semiconductor microcrystals," *Solid State Communications*, vol. 88, no. 11-12, pp. 947–950, 1993.

[42] N. F. Borrelli, D. Hall, H. Holland, and D. Smith, "Quantum confinement effects of semiconducting microcrystallites in glass," *Journal of Applied Physics*, vol. 61, no. 12, pp. 5399–5409, 1987.

[43] N. Gaponik, D. V. Talapin, A. L. Rogach, *et al.*, "Thiol-capping of cdte nanocrystals: An alternative to organometallic synthetic routes," *The Journal of Physical Chemistry B*, vol. 106, no. 29, pp. 7177–7185, 2002.

[44] M. V. Kovalenko, M. Scheele, and D. V. Talapin, "Colloidal nanocrystals with molecular metal chalcogenide surface ligands," *Science*, vol. 324, no. 5933, pp. 1417–1420, 2009.

[45] J. Zhang, J. Gao, C. P. Church, *et al.*, "Pbse quantum dot solar cells with more than 6% efficiency fabricated in ambient atmosphere," *Nano Letters*, vol. 14, no. 10, pp. 6010–6015, 2014.

[46] O. E. Semonin, J. M. Luther, S. Choi, *et al.*, "Peak external photocurrent quantum efficiency exceeding 100% via meg in a quantum dot solar cell," *Science*, vol. 334, no. 6062, pp. 1530–1533, 2011.

[47] J. R. Manders, L. Qian, A. Titov, *et al.*, "High efficiency and ultra-wide color gamut quantum dot leds for next generation displays," *Journal of the Society for Information Display*, vol. 23, no. 11, pp. 523–528, 2015.

[48] B. Guzelturk, Y. Kelestemur, K. Gungor, *et al.*, "Stable and low-threshold optical gain in cdse/cds quantum dots: An all-colloidal frequency up-converted laser," *Advanced Materials*, vol. 27, no. 17, pp. 2741–2746, 2015.

[49] J. Roh, Y.-S. Park, J. Lim, and V. I. Klimov, "Optically pumped colloidal-quantum-dot lasing in led-like devices with an integrated optical cavity," *Nature Communications*, vol. 11, no. 1, p. 271, 2020.

[50] R. Yu, T. Ren, K. Sun, Z. Feng, G. Li, and C. Li, "Shape-controlled copper selenide nanocubes synthesized by an electrochemical crystallization method," *The Journal of Physical Chemistry C*, vol. 113, no. 25, pp. 10 833–10 837, 2009.

[51] D. V. Talapin, J. H. Nelson, E. V. Shevchenko, S. Aloni, B. Sadtler, and A. P. Alivisatos, "Seeded growth of highly luminescent cdse/cds nanoheterostructures with rod and tetrapod morphologies," *Nano Letters*, vol. 7, no. 10, pp. 2951–2959, 2007.

[52] B. Mahler, B. Nadal, C. Bouet, G. Patriarche, and B. Dubertret, "Core/shell colloidal semiconductor nanoplatelets," *Journal of the American Chemical Society*, vol. 134, no. 45, pp. 18 591–18 598, 2012.

[53] A. Prudnikau, A. Chuvilin, and M. Artemyev, "Cdse–cds nanoheteroplatelets with efficient photoexcitation of central cdse region through epitaxially grown cds wings," *Journal of the American Chemical Society*, vol. 135, no. 39, pp. 14 476–14 479, 2013.

[54] M. Bawendi, A. Kortan, M. Steigerwald, and L. Brus, "X-ray structural characterization of larger cdse semiconductor clusters," *The Journal of Chemical Physics*, vol. 91, no. 11, pp. 7282–7290, 1989.

[55] Y. Gao and P. Yin, "Synthesis of cubic cdse nanocrystals and their spectral properties," *Nanomaterials and Nanotechnology*, vol. 7, p. 1 847 980 417 701 747, 2017.

[56] Y. Kelestemur, D. Dede, K. Gungor, C. F. Usanmaz, O. Erdem, and H. V. Demir, "Alloyed heterostructures of cdse x s1–x nanoplatelets with highly tunable optical gain performance," *Chemistry of Materials*, vol. 29, no. 11, pp. 4857–4865, 2017.

[57] K. Yusuf, G. Burak, E. Onur, *et al.*, "Cdse/cdse1–xtex core/crown hetero-nanoplatelets: Tuning the excitonic properties without changing the thickness," *The Journal of Physical Chemistry*, 2017.

[58] A. A. Rossinelli, H. Rojo, A. S. Mule, *et al.*, "Compositional grading for efficient and narrowband emission in cdse-based core/shell nanoplatelets," *Chemistry of Materials*, vol. 31, no. 22, pp. 9567–9578, 2019.

[59] B. T. Diroll, "Colloidal quantum wells for optoelectronic devices," *Journal of Materials Chemistry C*, vol. 8, no. 31, pp. 10 628–10 640, 2020.

[60] M. Sharma, K. Gungor, A. Yeltik, *et al.*, "Near-unity emitting copper-doped colloidal semiconductor quantum wells for luminescent solar concentrators," *Advanced Materials*, vol. 29, no. 30, p. 1 700 821, 2017.

[61] F. Fan, P. Kanjanaboos, M. Saravanapavanantham, *et al.*, "Colloidal cdse1–x s x nanoplatelets with narrow and continuously-tunable electroluminescence," *Nano Letters*, vol. 15, no. 7, pp. 4611–4615, 2015.

[62] C. She, I. Fedin, D. S. Dolzhnikov, *et al.*, "Red, yellow, green, and blue amplified spontaneous emission and lasing using colloidal cdse nanoplatelets," *ACS Nano*, vol. 9, no. 10, pp. 9475–9485, 2015.

[63] M. Liu, N. Yazdani, M. Yarema, M. Jansen, V. Wood, and E. H. Sargent, "Colloidal quantum dot electronics," *Nature Electronics*, vol. 4, no. 8, pp. 548–558, 2021.

[64] R. Rossetti, S. Nakahara, and L. E. Brus, "Quantum size effects in the redox potentials, resonance raman spectra, and electronic spectra of cds crystallites in aqueous solution," *The Journal of Chemical Physics*, vol. 79, no. 2, pp. 1086–1088, 1983.

[65] J. Caruge, J. E. Halpert, V. Wood, V. Bulović, and M. Bawendi, "Colloidal quantum-dot light-emitting diodes with metal-oxide charge transport layers," *Nature Photonics*, vol. 2, no. 4, pp. 247–250, 2008.

[66] Y. V. Vandyshev, V. Dneprovskii, V. Klimov, and D. Okorokov, "Lasing on a transition between quantum-well levels in a quantum dot," *Jetp Lett*, vol. 54, no. 8, p. 442, 1991.

[67] A. J. Nozik, "Quantum dot solar cells," *Physica E: Low-dimensional Systems and Nanostructures*, vol. 14, no. 1-2, pp. 115–120, 2002.

[68] G. Konstantatos, I. Howard, A. Fischer, *et al.*, "Ultrasensitive solution-cast quantum dot photodetectors," *Nature*, vol. 442, no. 7099, pp. 180–183, 2006.

[69] M. A. Boles, D. Ling, T. Hyeon, and D. V. Talapin, "The surface science of nanocrystals," *Nature Materials*, vol. 15, no. 2, pp. 141–153, 2016.

[70] M. A. Boles, M. Engel, and D. V. Talapin, "Self-assembly of colloidal nanocrystals: From intricate structures to functional materials," *Chemical Reviews*, vol. 116, no. 18, pp. 11 220–11 289, 2016.

[71] Y. Min, M. Akbulut, K. Kristiansen, Y. Golan, and J. Israelachvili, "The role of interparticle and external forces in nanoparticle assembly," *Nature Materials*, vol. 7, no. 7, pp. 527–538, 2008.

[72] C. Murray, C. Kagan, and M. Bawendi, "Self-organization of cdse nanocrystallites into three-dimensional quantum dot superlattices," *Science*, vol. 270, no. 5240, pp. 1335–1338, 1995.

[73] E. Rabani, "Structure and electrostatic properties of passivated cdse nanocrystals," *The Journal of Chemical Physics*, vol. 115, no. 3, pp. 1493–1497, 2001.

[74] J. N. Israelachvili, "Van der waals forces," *Intermolecular and Surface Forces*, pp. 107–132, 2011.

[75] E. Rabani, "An interatomic pair potential for cadmium selenide," *The Journal of Chemical Physics*, vol. 116, no. 1, pp. 258–262, 2002.

[76] B. Abécassis, "Self-assembly of colloidal semiconducting nanoplatelets," Ph.D. dissertation, Université Paris Sud Orsay, 2016.

[77] A. Böker, J. He, T. Emrick, and T. P. Russell, "Self-assembly of nanoparticles at interfaces," *Soft Matter*, vol. 3, no. 10, pp. 1231–1248, 2007.

[78] M. Grzelczak, J. Vermant, E. M. Furst, and L. M. Liz-Marzán, "Directed self-assembly of nanoparticles," *ACS Nano*, vol. 4, no. 7, pp. 3591–3605, 2010.

[79] P. L. Saldanha, V. Lesnyak, and L. Manna, "Large scale syntheses of colloidal nanomaterials," *Nano Today*, vol. 12, pp. 46–63, 2017.

[80] J. Yang, R. Fainblat, S. G. Kwon, *et al.*, "Route to the smallest doped semiconductor: Mn2+-doped (cdse) 13 clusters," *Journal of the American Chemical Society*, vol. 137, no. 40, pp. 12 776–12 779, 2015.

[81] G. H. Bertrand, A. Polovitsyn, S. Christodoulou, A. H. Khan, and I. Moreels, "Shape control of zincblende cdse nanoplatelets," *Chemical Communications*, vol. 52, no. 80, pp. 11 975–11 978, 2016.

[82] D. V. Talapin, E. V. Shevchenko, C. B. Murray, A. Kornowski, S. Förster, and H. Weller, "Cdse and cdse/cds nanorod solids," *Journal of the American Chemical Society*, vol. 126, no. 40, pp. 12 984–12 988, 2004.

[83] B. Abécassis, M. D. Tessier, P. Davidson, and B. Dubertret, "Self-assembly of cdse nanoplatelets into giant micrometer-scale needles emitting polarized light," *Nano Letters*, vol. 14, no. 2, pp. 710–715, 2014.

[84] K. Bian, R. Li, and H. Fan, "Controlled self-assembly and tuning of large pbs nanoparticle supercrystals," *Chemistry of Materials*, vol. 30, no. 19, pp. 6788–6793, 2018.

[85] D. V. Talapin and C. B. Murray, "Pbse nanocrystal solids for n-and p-channel thin film field-effect transistors," *Science*, vol. 310, no. 5745, pp. 86–89, 2005.

[86] T. P. Bigioni, X.-M. Lin, T. T. Nguyen, E. I. Corwin, T. A. Witten, and H. M. Jaeger, "Kinetically driven self assembly of highly ordered nanoparticle monolayers," *Nature Materials*, vol. 5, no. 4, pp. 265–270, 2006.

[87] O. Erdem and H. V. Demir, *Oriented Self-assembly of Colloidal Semiconductor Nanoplatelets on Liquid Interfaces: Methods and Applications*. Springer Nature, 2022.

[88] A. Dong, J. Chen, S. J. Oh, *et al.*, "Multiscale periodic assembly of striped nanocrystal superlattice films on a liquid surface," *Nano Letters*, vol. 11, no. 2, pp. 841–846, 2011.

[89] A. Dong, J. Chen, P. M. Vora, J. M. Kikkawa, and C. B. Murray, "Binary nanocrystal superlattice membranes self-assembled at the liquid–air interface," *Nature*, vol. 466, no. 7305, pp. 474–477, 2010.

[90] B. Peng, G. Li, D. Li, *et al.*, "Vertically aligned gold nanorod monolayer on arbitrary substrates: Self-assembly and femtomolar detection of food contaminants," *ACS Nano*, vol. 7, no. 7, pp. 5993–6000, 2013.

[91] H. D. Baruj, I. Bozkaya, B. Canimkurbey, *et al.*, "Highly-directional, highly-efficient solution-processed light-emitting diodes of all-face-down oriented colloidal quantum well self-assembly," *Small*, p. 2 206 582, 2023.

[92] R. Scott, J. Heckmann, A. V. Prudnikau, *et al.*, "Directed emission of cdse nanoplatelets originating from strongly anisotropic 2d electronic structure," *Nature Nanotechnology*, vol. 12, no. 12, pp. 1155–1160, 2017.